SANDIA REPORT

SAND2011-5529
Unlimited Release

Simulation of One-Minute Power Output from Utility-Scale Photovoltaic Generation Systems

Clifford W. Hansen, Joshua S. Stein, Abraham Ellis

Prepared by
Sandia National Laboratories
Albuquerque, New Mexico 87185 and Livermore, California 94550

Sandia National Laboratories is a multi-program laboratory managed and operated by Sandia Corporation,
a wholly owned subsidiary of Lockheed Martin Corporation, for the U.S. Department of Energy's
National Nuclear Security Administration under contract DE-AC04-94AL85000.

Approved for public release; further dissemination unlimited.

Sandia National Laboratories

Issued by Sandia National Laboratories, operated for the United States Department of Energy by Sandia Corporation.

NOTICE: This report was prepared as an account of work sponsored by an agency of the United States Government. Neither the United States Government, nor any agency thereof, nor any of their employees, nor any of their contractors, subcontractors, or their employees, make any warranty, express or implied, or assume any legal liability or responsibility for the accuracy, completeness, or usefulness of any information, apparatus, product, or process disclosed, or represent that its use would not infringe privately owned rights. Reference herein to any specific commercial product, process, or service by trade name, trademark, manufacturer, or otherwise, does not necessarily constitute or imply its endorsement, recommendation, or favoring by the United States Government, any agency thereof, or any of their contractors or subcontractors. The views and opinions expressed herein do not necessarily state or reflect those of the United States Government, any agency thereof, or any of their contractors.

Printed in the United States of America. This report has been reproduced directly from the best available copy.

Available to DOE and DOE contractors from
U.S. Department of Energy
Office of Scientific and Technical Information
P.O. Box 62
Oak Ridge, TN 37831

Telephone: (865) 576-8401
Facsimile: (865) 576-5728
E-Mail: reports@adonis.osti.gov
Online ordering: http://www.osti.gov/bridge

Available to the public from
U.S. Department of Commerce
National Technical Information Service
5285 Port Royal Rd.
Springfield, VA 22161

Telephone: (800) 553-6847
Facsimile: (703) 605-6900
E-Mail: orders@ntis.fedworld.gov
Online order: http://www.ntis.gov/help/ordermethods.asp?loc=7-4-0#online

SAND2011-5529
Unlimited Release

Simulation of One-Minute Power Output from Utility-Scale Photovoltaic Generation Systems

Clifford W. Hansen, Joshua S. Stein, Abraham Ellis
Photovoltaics and Grid Integration Department
Sandia National Laboratories
P.O. Box 5800
Albuquerque, New Mexico 87185-MS1033

Abstract

We present an approach to simulate time-synchronized, one-minute power output from large photovoltaic (PV) generation plants in locations where only hourly irradiance estimates are available from satellite sources. The approach uses one-minute irradiance measurements from ground sensors in a climatically and geographically similar area. Irradiance is translated to power using the Sandia Array Performance Model. Power output is generated for 2007 in southern Nevada are being used for a Solar PV Grid Integration Study to estimate the integration costs associated with various utility-scale PV generation levels. Plant designs considered include both fixed-tilt thin-film, and single-axis-tracked polycrystalline Si systems ranging in size from 5 to 300 MW_{AC}. Simulated power output profiles at one-minute intervals were generated for five scenarios defined by total PV capacity (149.5 MW, 222 WM, 292 MW, 492 MW, and 892 MW) each comprising as many as 10 geographically separated PV plants.

ACKNOWLEDGMENTS

NV Energy provided the hypothetical plants and scenarios summarized in Figure 1 and Table 1. The Las Vegas Valley Water District provided measured one-minute irradiance data from several sensors within the Las Vegas valley as indicated in Figure 3.

We are grateful for the external reviews provided by Mr. Matthew Lave of the University of California at San Diego, and by Dr. Marissa Hummon of the National Renewable Energy Laboratory.

CONTENTS

1. Introduction 9

2. Methodology 11
  2.1 Estimation of One-Minute Point Irradiance at Study Sites 13
    2.1.1 Available Irradiance Data 13
    2.1.2 Review of Downscaling Methods 14
    2.1.3 Selected Downscaling Approach 16
  2.3 Estimation of Spatially-Averaged Irradiance at Study Sites 17
  2.4 Translation to Plane-of-Array Irradiance 19
  2.5 Calculation of One-Minute AC Power Output 20

3. Results 21
  3.1 Illustrative Results 21
  3.2. Validation 23
    3.2.1. Distributions of Irradiance 24
    3.2.2. Distributions of Changes in Irradiance 24
    3.2.3. Correlations Between Changes in Irradiance 26

4. Ancillary Analyses 29
  4.1. Day-ahead Forecasts 29
    Step 1: Classify each day of the year as clear or cloudy. 30
    Step 2: Generate forecast values for clear days. 32
    Step 3: Generate forecast values for cloudy days. 32
  4.2. Power from Distributed PV Systems 35

4. References 39

Distribution [can go on an even or an odd page] 41

FIGURES

Figure 1. Map showing locations for hypothetical PV plants considered in the study. 9
Figure 2. Relationship between irradiance and AC power from the entire La Ola plant for April 1, 2010, a partly cloudy day. 12
Figure 3. Map of LVVWD sites with one-minute irradiance measurements. 13
Figure 4. Comparison of satellite (red) and the best fit one-minute irradiance day. 17
Figure 5. Distribution of calculated upper air wind speed from Desert Rock station for 2007... 18
Figure 6. Comparison of one-minute point irradiance and estimated spatial average irradiance for two different plant sizes: 50 MW (left) and 300 MW (right). 19
Figure 7. One Week of Estimated Irradiance and Power for Site 1, Case 5 (20MW). 21
Figure 8. Estimated Irradiance at all Sites on Day 202 22
Figure 9. Estimated AC Power at all Sites on Day 202, Case 5. 23
Figure 10. Comparison of CDFs of Annual Irradiance Between Simulated One-Minute Irradiance and Hourly Average Irradiance Estimated From Satellite Data. 25
Figure 11. Comparison of CDFs of Changes in One-Minute Irradiance Between Simulations and LVVWD Data. 26

Figure 12. Correlations between Changes in Clear Sky Index (Kt) as a Function of Distance between Sites and Time Interval. 28
Figure 13. Identification of Clear and Cloudy Days. 30
Figure 14. Occurrence of Clear and Cloudy Days in 2007. 31
Figure 15. Irradiance Patterns on Clear and Cloudy Days. 31
Figure 16. Sampled Relative Forecast Errors for Clear Days (blue) and Target Error Distribution (red). 33
Figure 17. Forecast Error for Cloudy Days as a Function of Clear Sky Index. 34
Figure 18. Comparison of Simulated Irradiance to Day-Ahead Forecast. 35
Figure 19. Comparison of Actual and Forecast GHI: Emulated Forecast (left) and Numerical Weather Model-Based Forecast for Desert Rock, Nevada (right). 36
Figure 20. One Week of Estimated Power from Distributed Generation PV. 37

TABLES

Table 1. PV Plant Sizes (MW_{AC}) for each Scenario 10
Table 2. Irradiance Data Available from LVVWD Ground Measurements. 14
Table 3. Plant area per MW_{AC}. 17
Table 4. Parameters and Values for Clear Sky Model 27
Table 5. Standard Deviations Used to Generate Relative Forecast Errors for Cloudy Days. 33
Table 6. Summary of Distributed Generation PV Cases. 36

NOMENCLATURE

CDF	Cumulative distribution function
DC	Direct current
DG	Distributed generation
DNI	Direct normal irradiance
DOE	Department of Energy
GHI	Global horizontal irradiance
LVVWD	Las Vegas Valley Water District
kW_{AC}	Kilowatt AC power
MW	Megawatt
MW_{AC}	Megawatt AC power
NV	Nevada
POA	Plane of array
PV	Photovoltaic
RMSE	Root mean square error
SNL	Sandia National Laboratories

1. INTRODUCTION

NV Energy balances load and generation for most of the state of Nevada. In July 2010 the Public Utility Commission of Nevada requested that NV Energy study how different levels of photovoltaic (PV) generation would affect load balancing for the utility [1]. Sandia National Laboratories (SNL) participated in this study by producing time-synchronized, one-minute PV output profiles for proposed PV plants at 10 locations across southern Nevada (Figure 1). Five scenarios were considered, varying in the number of plants and the size of each plant, and ranging from 149.5 MW up to 892 MW total PV capacity. The scenarios and their constituent hypothetical PV plants are summarized in Table 1.

Simulations were performed using satellite estimates and ground measurements of irradiance, as well as temperature and wind speed recordings for 2007; this year was selected for the study period because of the availability of data and because NV Energy recorded its highest peak load during that summer. NV Energy and its consultant, Navigant Consulting, used these profiles to calculate the effect on balancing operations (e.g., additional load following and regulation reserves) of various levels of utility-scale PV generation. NV Energy's study and findings are reported in Navigant, 2011 [2].

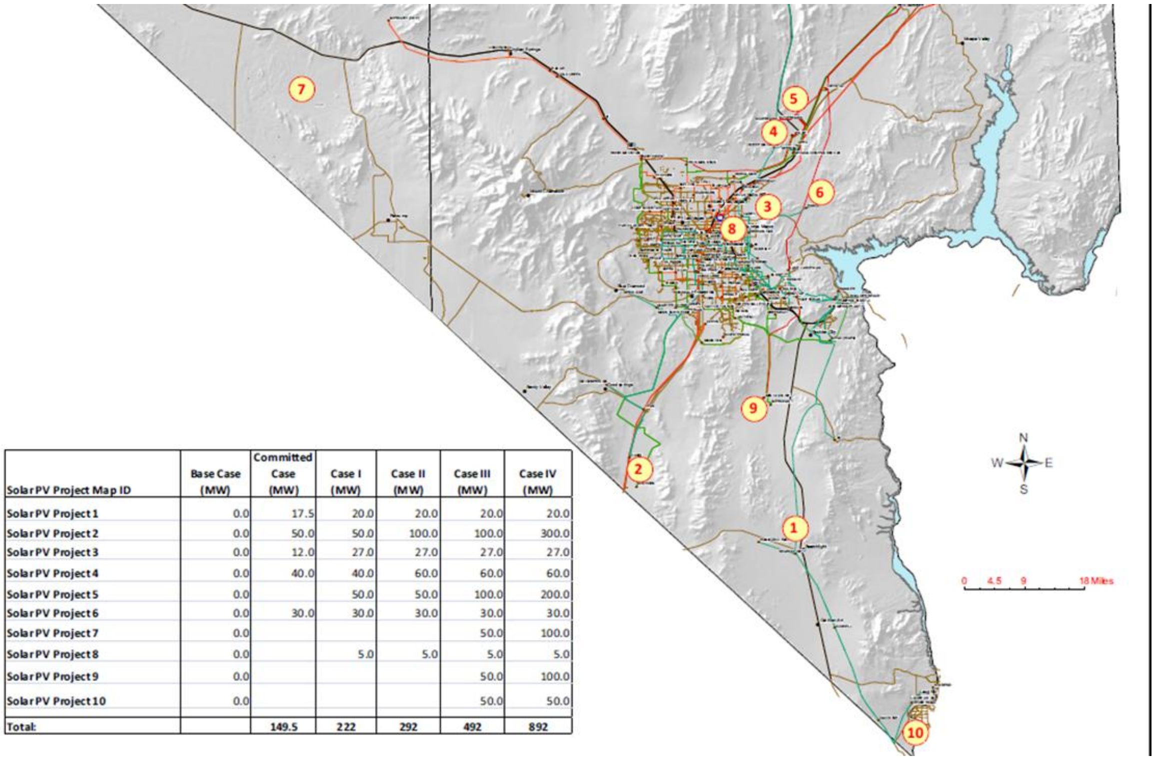

Solar PV Project Map ID	Base Case (MW)	Committed Case (MW)	Case I (MW)	Case II (MW)	Case III (MW)	Case IV (MW)
Solar PV Project 1	0.0	17.5	20.0	20.0	20.0	20.0
Solar PV Project 2	0.0	50.0	50.0	100.0	100.0	300.0
Solar PV Project 3	0.0	12.0	27.0	27.0	27.0	27.0
Solar PV Project 4	0.0	40.0	40.0	60.0	60.0	60.0
Solar PV Project 5	0.0		50.0	50.0	100.0	200.0
Solar PV Project 6	0.0	30.0	30.0	30.0	30.0	30.0
Solar PV Project 7	0.0				50.0	100.0
Solar PV Project 8	0.0		5.0	5.0	5.0	5.0
Solar PV Project 9	0.0				50.0	100.0
Solar PV Project 10	0.0				50.0	50.0
Total:		149.5	222	292	492	892

Figure 1. Map showing locations for hypothetical PV plants considered in the study.

Table 1. PV Plant Sizes (MW_{AC}) for each Scenario

	Scenario				
Site	**S1**	**S2**	**S3**	**S4**	**S5**
1	17.5	20	20	20	20
2*	50	50	100	100	300
3*	12	27	27	27	27
4	40	40	60	60	60
5*	-	50	50	100	200
6	30	30	30	30	30
7	-	-	-	50	100
8*	-	5	5	5	5
9*	-	-	-	50	100
10	-	-	-	50	50
Scenario Total (MW_{AC})	149.5	222	292	492	892

* Indicates PV plants that are specified to be latitude tilt, thin-film modules. Other plants are specified to be single axis tracking, polycrystalline Si modules

In this report, we document our method for simulating one-minute time series of power for each of the utility-scale plants listed in Table 1. We describe our simulation method in Section 2; results are illustrated in Section 3, along with evidence for validity of the simulation results.

The grid integration study documented in [2] also required day-ahead forecasts (at hourly time steps) of power from utility-scale plants. Forecasts were emulated by applying random error to our time series of power from each plant. We reviewed the literature to identify a reasonable characterization of forecast errors that may result when using current forecasting methods. Our method for emulating forecasts is described in Section 4.1.

In addition, the grid integration study required one-minute time series of aggregate power from small commercial (i.e., less than $3MW_{AC}$) and residential PV systems distributed throughout the Las Vegas valley. We estimated these time series using a simplified version of our simulation approach, as described in Section 4.2.

2. METHODOLOGY

The instantaneous power output from a PV plant is determined by a number of factors, including: module and inverter characteristics; irradiance over the plant area; temperature of the PV cells; angle of incidence and spectral quality of the light; and losses, including soiling, wiring, and conversion losses.

Based on many years of outdoor module and array testing, Sandia has developed the Sandia PV Array Performance Model [3], which estimates instantaneous direct current (DC) power output from a PV module, given irradiance, angle of incidence, absolute air mass (i.e., the optical path length through the atmosphere, relative to solar zenith at sea level), ambient air temperature and wind speed. One challenge of applying this and other PV performance models to large PV systems is that the models generally expect a single value of irradiance as input. As PV systems become larger it is more likely that irradiance will vary spatially over the plant as cloud shadows pass over parts of the plant's footprint.

Studies performed by Sandia at the La Ola 1.2 MW PV plant in Lanai, HI [4] have illustrated the relationship between plant output and irradiance measured by a network of irradiance sensors spread over the plant footprint. The study results show that short-term (i.e., one-second) power output from a PV plant is approximately proportional to the spatial average of plane-of-array (POA) irradiance over the plant footprint. Figure 2 shows a scatterplot of one-second AC power from the plant against POA irradiance from several single sensors (red dots) and the spatial average of POA irradiance (blue dots) determined from all 16 sensors distributed within the plant area. Scatterplots between power and POA irradiance measured at other single sensors are similar to the red dots in Figure 2. The heavy black line indicates AC power as a function of irradiance that would result from using the Sandia PV Array Performance Model and applying the spatial average POA irradiance uniformly over the plant area. Excursions of the single sensor data (red dots) from the black line indicate periods of time when POA irradiance at the single sensor differed substantially from the spatial average irradiance over the plant area, due to the presence of cloud shadows over part, but not all, of the plant's area.

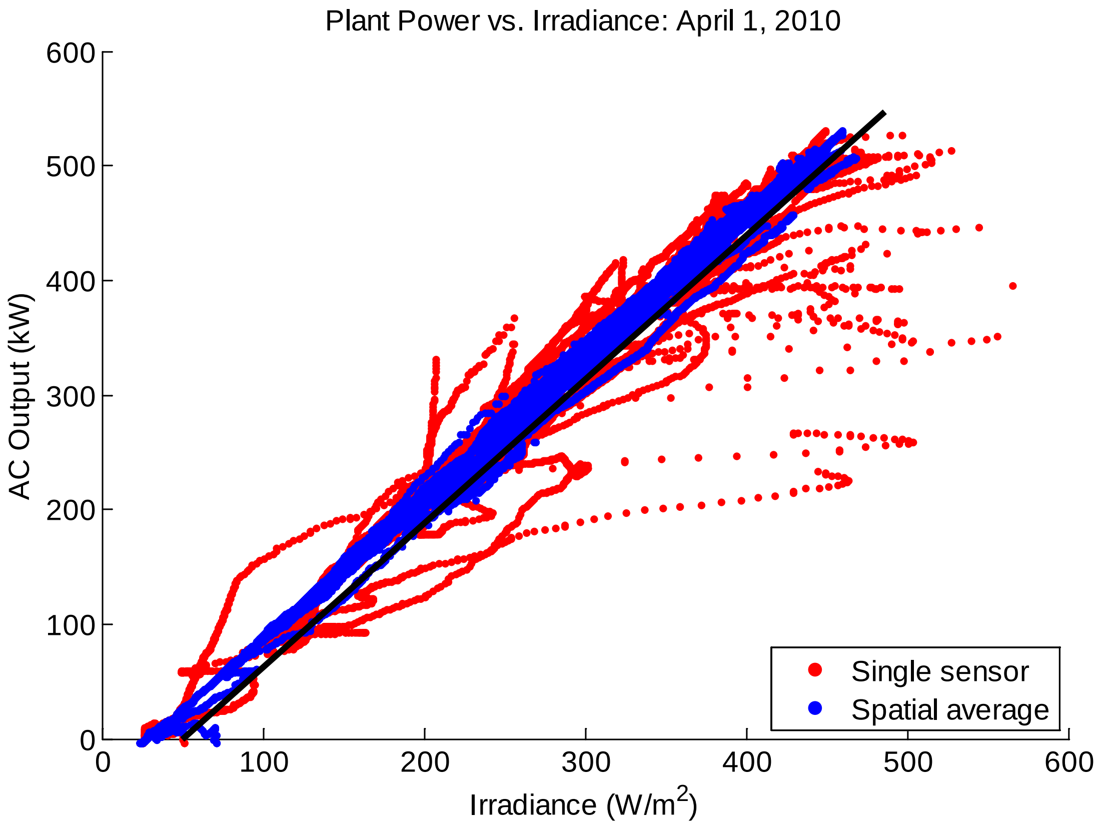

Figure 2. Relationship between irradiance and AC power from the entire La Ola plant for April 1, 2010, a partly cloudy day.

It is apparent from Figure 2 that power output is better correlated with the spatial average of POA irradiance than with irradiance from a single sensor. The correlation between the spatial average of POA irradiance and power is observed across the range of irradiance and thus holds for both clear and cloudy conditions, implying that the spatial average of POA irradiance can be used in the PV performance model to predict power for all conditions.

Accordingly, our method broadly focuses on estimating one-minute spatial average of POA irradiance at the locations of each hypothetical PV plant, consistent with available information about irradiance at those locations. The spatial average of POA irradiance is then used in the Sandia PV Array Performance Model to estimate power from each plant.

The method is outlined below as a sequence of steps:

1. Estimating one-minute global horizontal irradiance at a point at each study site;
2. Estimating spatially-averaged global horizontal irradiance over the footprint of each hypothetical PV plant;
3. Translating spatially-averaged global horizontal irradiance to spatially-averaged POA irradiance;
4. Calculation of one-minute AC power output.

2.1 Estimation of One-Minute Point Irradiance at Study Sites

Estimation of one-minute point irradiance involved downscaling (in time) from hourly information to one-minute time series. We discuss here: available data; review of published downscaling methods that have been applied to irradiance; and our selected approach.

2.1.1 Available Irradiance Data

No ground measurements of irradiance were available at any of the locations of the hypothetical PV plants during 2007. However, one-minute averages of global horizontal irradiance were available from pyranometers at other locations, namely, six Las Vegas Valley Water District (LVVWD) installations within the Las Vegas valley, as shown in Figure 3, for the periods of time listed in Table 2.

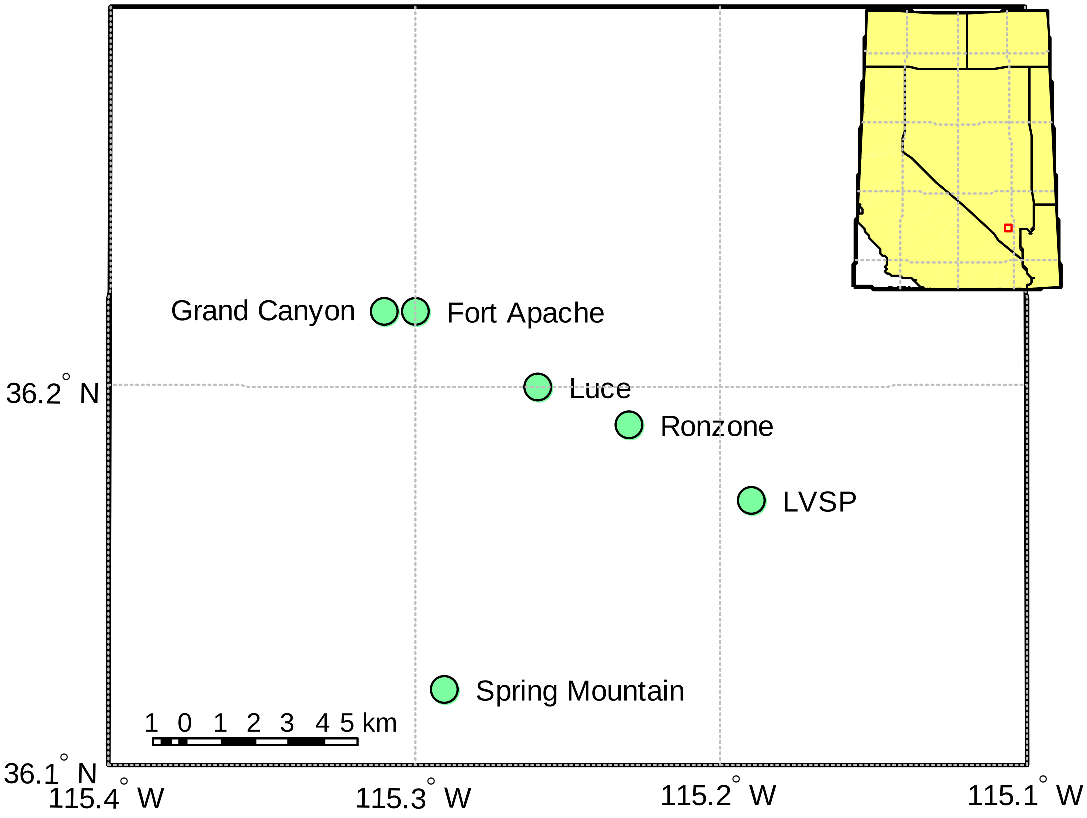
Grand Canyon
Fort Apache
Luce
Ronzone
LVSP
Spring Mountain
36.2° N
36.1° N
115.4° W
115.3° W
115.2° W
115.1° W
1 0 1 2 3 4 5 km

Figure 3. Map of LVVWD sites with one-minute irradiance measurements.

Table 2. Irradiance Data Available from LVVWD Ground Measurements.

Station Name	Location	Start Date for Data	End Date for Data
Fort Apache	36.22N 115.30W	8/23/2006	4/29/2009
Grand Canyon	36.22N 115.31W	9/30/2006	4/29/2009
Las Vegas Springs Preserve	36.17N 115.19W	7/26/2007	4/29/2009
Spring Mountain	36.12N 115.29W	11/30/2006	4/29/2009
Luce	36.20N 115.26W	5/2/2007	4/29/2009
Ronzone	36.19N 115.23W	4/27/2006	4/29/2009

Estimates of irradiance at hourly intervals on a 10×10 km grid for the entire United States are available through the SolarAnywhere service from Clean Power Research [5]. This data is currently provided free of charge for time periods older than 3 years. Irradiance is estimated from GOES satellite imagery using algorithms developed by Perez and others [6]. These algorithms have been validated by several researchers [7-9]. Irradiance estimates at hourly intervals for the 10 study sites were obtained. These estimates represent instantaneous irradiance over a single satellite pixel (~1 km^2), which is somewhere in the 10×10 km area. Variability in the geopositioning of individual pixels can be as great as several kilometers between images. Lacking any other information about irradiance at each site, we viewed the satellite-derived irradiance values as instantaneous estimates of irradiance at each site. The satellite-derived irradiance values were used to calculate hourly averages of irradiance by averaging the two measurements which span the hour (the start and end of the hour).

2.1.2 Review of Downscaling Methods

To downscale from hourly average irradiance to one-minute irradiance at each site, we considered several options. We first reviewed a number of irradiance simulation models which aim to simulate time series of irradiance. These models generally simulate time-series of clear sky index, i.e., irradiance divided by clear sky irradiance. Histograms of clear sky index values are generally bimodal when the time intervals are short (e.g., one-minute), reflecting clear and cloudy conditions.

An approach suggested by Glasbey [10] involves simulating clear sky index as a nonlinear autoregressive time series with the joint distributions of clear sky index at lag one defined by multivariate Gaussian mixtures. Components of the mixture are interpreted as representing different cloud conditions: clear skies; intermittent cloudy skies; and overcast conditions. Glasbey reports fitting the model to data from northeast Scotland and showed that simulated time-series reasonably reproduce the histogram of clear sky index over time, and scatterplots of clear sky index vs. lagged clear sky index. We fit the proposed model form to data from LVVWD and used the fitted model to simulate time series of one-minute irradiance. We found that the variance in the simulated irradiance was generally higher than observed in the ground-based irradiance measurements. We attribute the higher variance to the low lag (i.e., one minute) considered in the fitted models, which appears to be too low to reproduce longer-period features evident in the LVVWD time series. In particular, the LVVWD data show many clear hours, interrupted by relatively infrequent periods of variable irradiance, and occasionally, by longer periods (i.e., several hours) of overcast conditions. The low lag causes the simulations to switch between mixture components too frequently. Using the fitted model to produce time series of irradiance for the NV Energy study would result in more frequent and/or larger ramps in simulated power than are supported by available data. We did not consider modifying the model form to introduce higher order lags.

Skartveit and Olseth [11] proposed a method to simulate five-minute clear sky index from hourly average values determined by data. For each hour, they construct a distribution of five-minute clear sky index values, sample from this distribution for each five-minute interval, and permute the sampled values to obtain a time series with lag one autocorrelation approximately equal to a target value. Each hour's distribution of five-minute clear sky index values is modeled as a mixture of two beta distributions, the parameters of which are derived from the hourly clear sky index, an estimate of the standard deviation of five-minute clear sky index within the hour, and by matching characteristics of a training sample comprising five-minute average irradiance data from Atlanta, GA, San Antonio, TX, and Geneva, Switzerland. The estimated intra-hour standard deviation is sampled from a Wiebull distribution, the parameters for which are given by empirically equations resulting from the training sample. The model is tested by comparing simulated time series against five-minute irradiance collected at Payerne, Switzerland, from which the target autocorrelation was also obtained. The authors present two sets of histograms of clear sky index, one conditional on solar elevation angle and a second conditional on average hourly clear sky index, to show that the model acceptably matches the target data.

We considered but did not pursue using the Skartveit and Olseth model because of the low order lag used to account for autocorrelations. We believe that, if this model form were fit to the LVVWD data, that the simulated time series would exhibit higher variability than observed in the data, for the same reasons that simulated time series obtained using the Glasbey model were too variable. We did not consider revising the Skartveit and Olseth model to introduce higher order temporal correlations.

Tovar and others [12-15] have identified relationships between the frequency distribution of clear sky index and other quantities such as the air mass and hourly average irradiance but do not specify a method for simulating time series. Essentially, these publications document various distribution forms that model the histogram of clear sky index, conditional on values for other quantities such as air mass. Results in these papers are conceptually similar to Skartveit and Olseth [11], who use a mixture of beta distributions to describe the frequency distribution of clear sky index conditional on hourly average clear sky index, and to Glasbey [10], who effectively models clear sky index using a mixture of Gaussian distributions. However, Tovar et al. [12-15] do not provide methods to account for temporal correlations (of relatively high order) in the time series of clear sky index. Consequently, simulations using their models would likely prove too variable, as we found for simulations using Glasbey's model, and anticipate would have resulted using the model of Skartveit and Olseth. Consequently, we did not pursue simulating time series using, in some manner, the distributions described by Tovar and others.

2.1.3 Selected Downscaling Approach

Instead of simulating time series of irradiance, we selected an approach that replays recorded irradiance in a manner that: 1) closely reproduces the frequency distribution of hourly average irradiance, as determined from satellite observations; 2) results in one-minute time series of irradiance with variability similar to that observed at the LVVWD sites; and 3) honors any spatial and/or seasonal patterns that might exist in the hourly averages. Our method starts by assembling a library of more than 5,000 one-day sequences of irradiance at one-minute intervals using all available ground station data (Table 2). We calculated the hourly average irradiance for each day in the library. Next, for each day at each of the 10 study sites, we calculated the sum of the squared differences (SSD) between the target irradiance (hourly averages from satellite data) and the hourly average of irradiance for each of the library days. We then sorted the library days and kept track of the 10 library days with the lowest SSD (best fit) for each day of 2007 and at each site.

The next step involved assigning a library irradiance day (comprising a time-series of one-minute irradiance) to each site for each day of the year. To prevent the same library day being assigned to more than one site on the same day of the year, we generated a random permutation of 1 to 10 for each day of the year. The permutation determined the order in which we assigned library days to the sites. For example, if the first four integers were 4, 1, 9, 2, … for a particular day, we began at Site 4 and chose the library day with the lowest SSD for that site and day. Next we examined Site 1. If the library day chosen for Site 4 also had the lowest SSD for Site 1, we chose the library day for Site 1 that had the second lowest SSD. We considered the remaining sites in the order specified by that day's permutation until each site was assigned a library day. Then we proceeded to the next day of the year and repeated the procedure. The permutation process ensures that the selection algorithm does not produce one-minute irradiance that is perfectly correlated between two sites on the same day. Figure 4 shows an example of the satellite irradiance for a day and the one-minute irradiance day from the library that was chosen.

The ground-based measurements of irradiance used to assign irradiance days to each plant location represent point measurements rather than spatial averages. The next step is to estimate the spatial average irradiance over each plant footprint. For this study we considered five scenarios (149.5 MW, 222 WM, 292 MW, 492 MW, and 892 MW). Each of these scenarios was defined as a mix of PV plants of varying sizes at each of the 10 sites (Table 1).

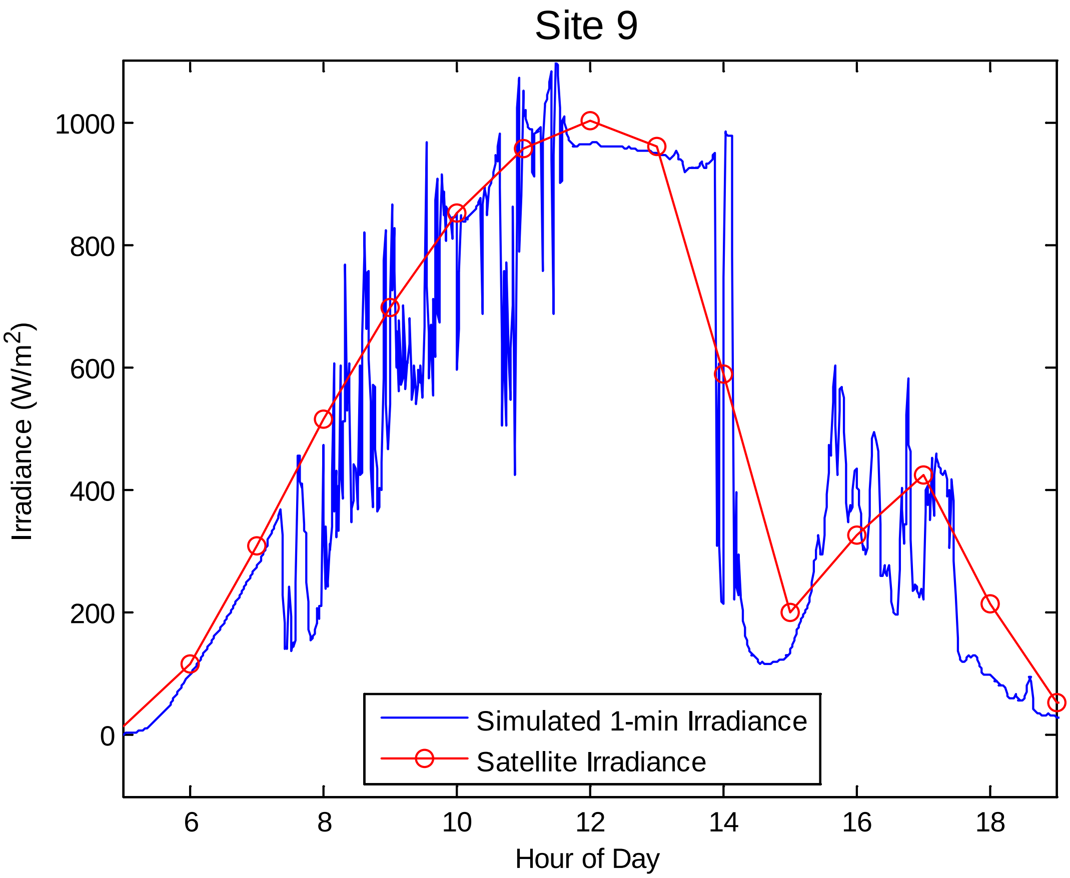

Figure 4. Comparison of satellite (red) and the best fit one-minute irradiance day.

2.3 Estimation of Spatially-Averaged Irradiance at Study Sites

Given a plant size (in MW_{AC}) and a technology (polycrystalline Si or thin-film), we made assumptions to estimate the total land area required (Table 3). For each plant listed in Table 1, we calculated PV plant area as the product of the plant capacity (MW_{AC}) and the conversion factor (acres/MW_{AC}) from Table 3, depending on the plant type.

Table 3. Plant area per MW_{AC}.

Module Technology	Mounting Configuration	Land Requirements (acres/MW_{AC})
Polycrystalline Si	Single-axis tracking	10
Thin-Film	Fixed latitude tilt	12.5

To estimate the spatial average irradiance over each plant, we applied the methodology developed by Longhetto et al. [16]. This method assumes that the spatial average of irradiance over an area can be estimated as a time average of point measurements of irradiance with an averaging window equal to the time it takes for a cloud to pass over the array. We estimated the characteristic length of the plant as the square root of the plant area (i.e., we assumed plants are square). The velocity of the cloud shadows across the landscape was estimated from upper air wind speed measurements made by NOAA from weather balloons launched from the Desert Rock station in Mercury, NV [17]. These balloons are launched every 12 hours throughout the year. We estimated wind speeds at cloud level as the average of the wind speeds measured from 1,000 to 8,000 meters above sea level. Figure 5 shows the distribution of resulting upper air wind speeds for 2007 (mean = 6.2 m/s). We extended the periodic measurements into a one-minute time series by assuming that wind velocity was constant for five and one half hours after a measurement, then linearly interpolated over the succeeding hour to the next measured wind speed. Thus, wind speeds were constant for a total of eleven hours, and changed linearly over a period of one hour to the next constant value.

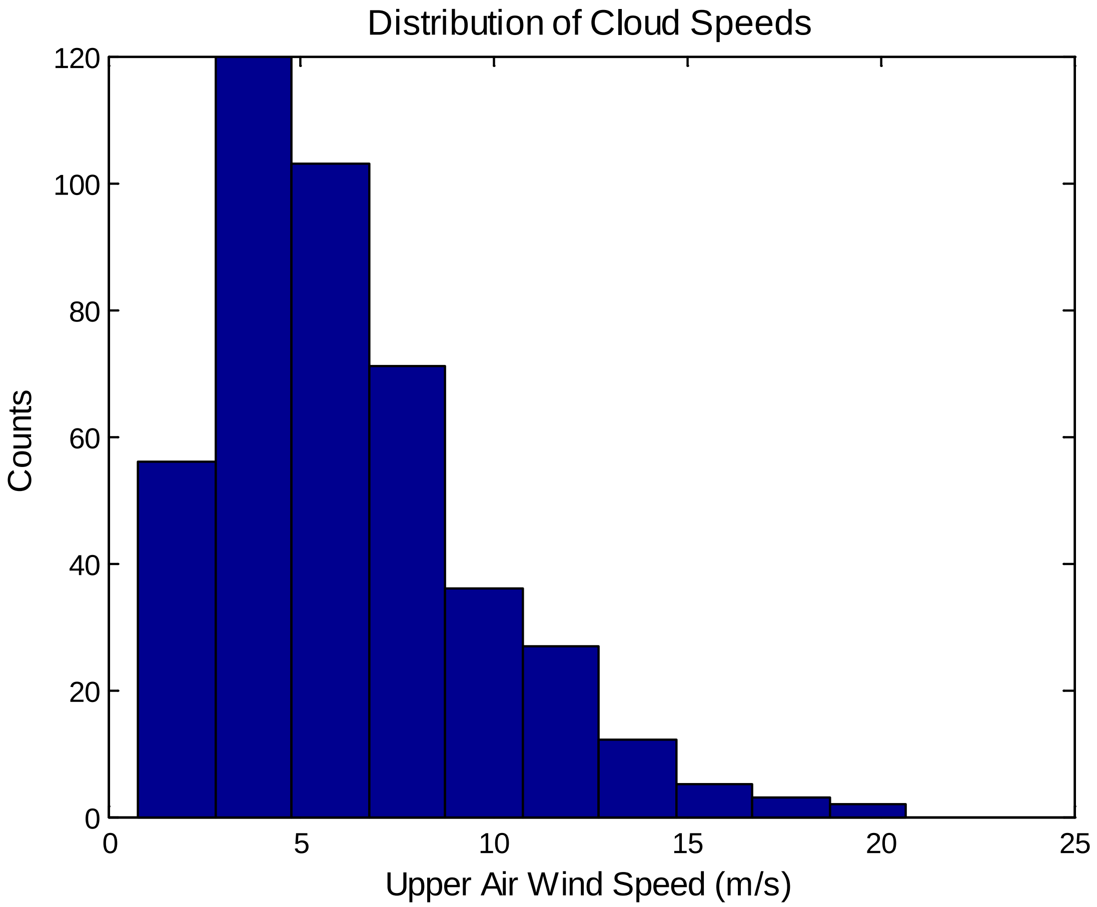

Figure 5. Distribution of calculated upper air wind speed from Desert Rock station for 2007.

Effectively, the method for spatial averaging outlined above resulting in averaging windows (in time) most commonly between two and five minutes. Infrequently, averaging windows exceeded five minutes, and rarely were greater than ten minutes. Figure 6 illustrates the reduction in the variability of irradiance resulting from averaging over the plant area. Greater reduction in variability is to be expected as plants become larger, due to the longer time required for cloud shadows to pass over the plant.

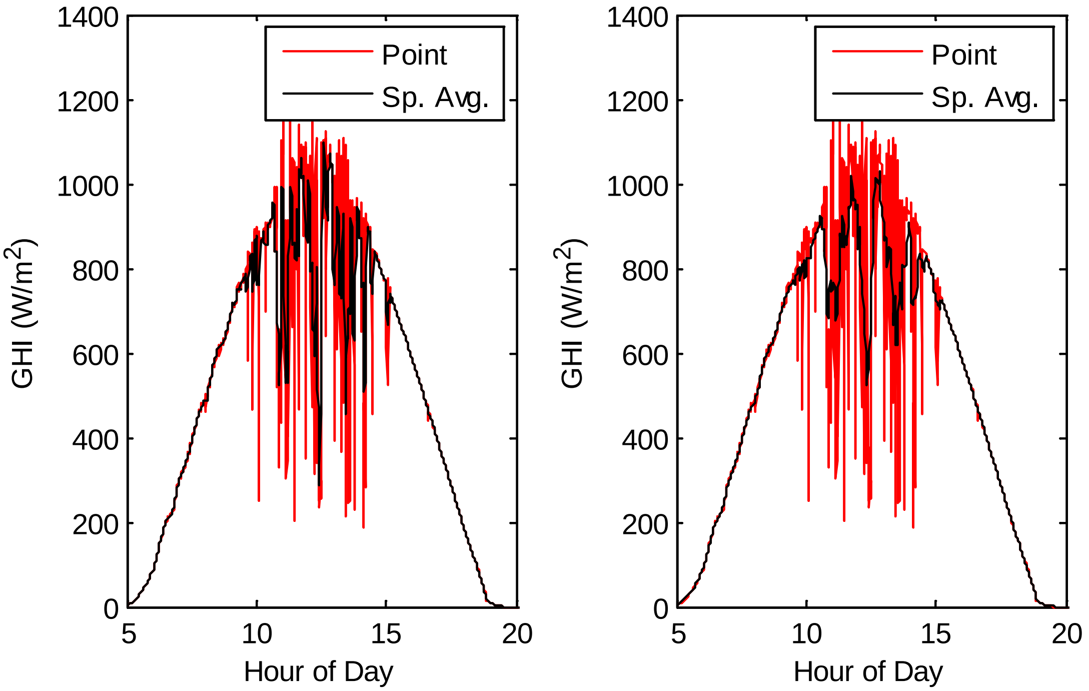

Figure 6. Comparison of one-minute point irradiance and estimated spatial average irradiance for two different plant sizes: 50 MW (left) and 300 MW (right).

2.4 Translation to Plane-of-Array Irradiance

To apply the Sandia PV Array Performance Model [3] we need to calculate the direct and diffuse components of POA irradiance. We applied the DISC model [18] to estimate the direct normal irradiance (DNI) from global horizontal irradiance (GHI) and calculated the diffuse (horizontal) as the difference: GHI - DNI × cos(Z), where Z is the zenith angle. The DISC model is based on empirical data collected across the U.S. relating the diffuse fraction to GHI. Beam irradiance at the POA is DNI × cos(AOI), where AOI is the angle of incidence between the sun and the module surface. The AOI is calculated from Eq 1:

$$AOI = \cos^{-1}\left[\begin{matrix} \cos(Z)\cos(T_a)+ \\ \sin(Z)\sin(T_a\cos(A_s - A_a) \end{matrix}\right], \tag{1}$$

where Z is the solar zenith angle, T_a is the tilt angle of the array, A_s is the solar azimuth angle (0°=North, 90°= East), and A_a is the array azimuth angle (0°=North, 90°= East).

In the case of the fixed (thin-film) arrays, AOI is simply a function of the solar zenith and azimuth angles, which vary with time. For single-axis tracked system (where the tracking axis is horizontal and oriented N-S), the tilt angle, array azimuth, and solar zenith angle vary with time. Eqs. 2 to 5 describe the calculation of the array tilt and azimuth angles, T_a and A_a for this configuration [19]:

$$\alpha = -\tan^{-1}\left[\frac{-\sin(Z)\sin(A_s)}{\cos(Z)}\right] \tag{2}$$

$$\beta = \begin{Bmatrix} T_m \\ -T_m \\ \alpha \end{Bmatrix} if \begin{Bmatrix} \alpha > T_m \\ \alpha < -T_m \\ else \end{Bmatrix} \tag{3}$$

where T_m is the maximum tilt angle for the tracker (assumed to be 45°).

$$T_a = |\beta| \tag{4}$$

$$A_a = \begin{Bmatrix} 90° \\ 270° \end{Bmatrix} if \begin{Bmatrix} \beta >= 0 \\ \beta < 0 \end{Bmatrix} \tag{5}$$

Diffuse irradiance on the POA was calculated using the translation model developed by Perez et al. [20]. The ground reflectance was assumed to be constant (0.2). It is assumed that there is no shading of the array.

2.5 Calculation of One-Minute AC Power Output

DC power output from each array was estimated by using the Sandia PV Array Performance Model [3] to calculate the maximum power point for each minute of the year. AC power was determined from DC power by using the Sandia PV Inverter Model [21]. We assumed that the polycrystalline Si plants are constructed using Yingli Solar YL230-29b modules and that thin film plants use First Solar FS-275 modules; either module is representative of currently available technology. Both types of plants were assumed to be divided into 500 $\mathrm{kW_{AC}}$ blocks and use SatCon PVS-500 (480$\mathrm{V_{AC}}$) inverters. We assume that inverter do not clip power, and that plant operators do not curtail output.

Modules are assumed to be connected with a sufficient number of series strings so that the product of the assumed DC derate factor of 0.85 and the DC rating of the modules is equal to the AC rating of the system (in MW). These technology assumptions were necessary in order to run the models but are not likely to affect the model results in a significant way, because the differences in AC power output from similar modules and inverters are relatively small in comparison to the variability in power output due to the variability in irradiance.

Cell temperature was estimated using the King model [3], which accounts for the effects of POA irradiance, air temperature and surface wind speed. Air temperature and surface wind speed were derived from weather data recorded at McCarran International Airport in Las Vegas, NV. Measured wind speeds were used at each site without adjustment, while measured air temperature data was lapse-adjusted for elevation differences between each site and the airport meteorological station.

3. RESULTS

The algorithm outlined in Section 2 was applied to generate one-minute time series of irradiance and power at each site contributing to each of the five scenarios summarized in Table 1. We first illustrate the irradiance and power results by examining a single site over several consecutive days, and all sites on the same day. We next compare simulation results to measured data as evidence of the simulation's validity; the comparisons examine the cumulative distributions of irradiance, cumulative distributions of changes in irradiance and correlations in the changes in irradiance as a function of distance between sites.

3.1 Illustrative Results

Figure 7 illustrates the relationship between estimated irradiance at a point on the ground at the site, and power from a 20MW total capacity plant, for one week, for Site 1 of Case 5. Both clear and cloudy periods are evident in the estimated irradiance. Power generally follows the estimated irradiance; cloudy periods exhibit varying irradiance and correspondingly variable power. Because Site 1 assumes single axis tracking, the power curves are squarer in shape than are the curves for irradiance.

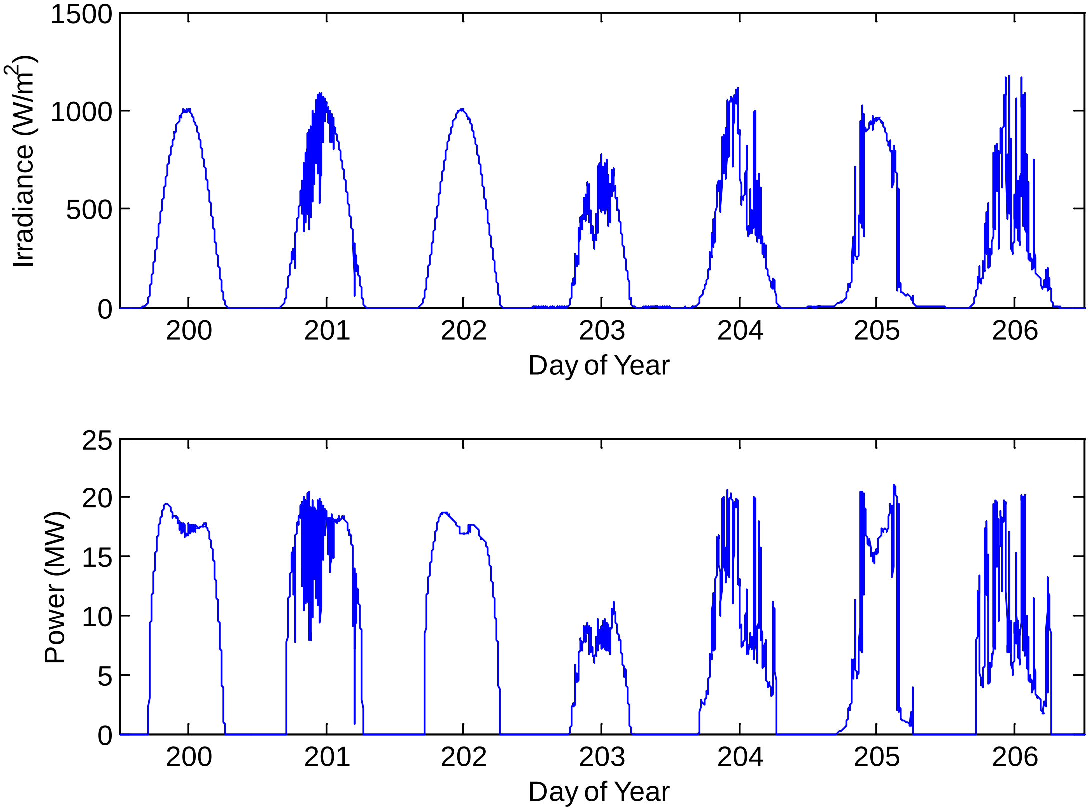

Figure 7. One Week of Estimated Irradiance and Power for Site 1, Case 5 (20MW).

Figure 8 compares irradiance at each site on the same day of the year (day 202). Hourly averages (estimated from satellite data) are indicated by the red circles; one-minute simulated irradiance is shown as blue lines. Figure 8 illustrates the reasonable match between the time series of hourly average irradiance and the simulated one-minute irradiance. The satellite estimate offer sufficient spatial resolution to distinguish different irradiance conditions at different sites (e.g., compare Site 1 and Site 2), and when the hourly averages of irradiance over the entire day depart sufficiently from clear sky conditions (e.g., compare Site 1 and Site 2), days with variable irradiance are selected from the library. However, if hourly averages indicate both clear and cloudy periods during the day (e.g., Site 9), the time series of one-minute irradiance may not reflect these periods, because one-minute irradiance is simulated by choosing an entire day from the library, rather than mixing periods of irradiance from different days.

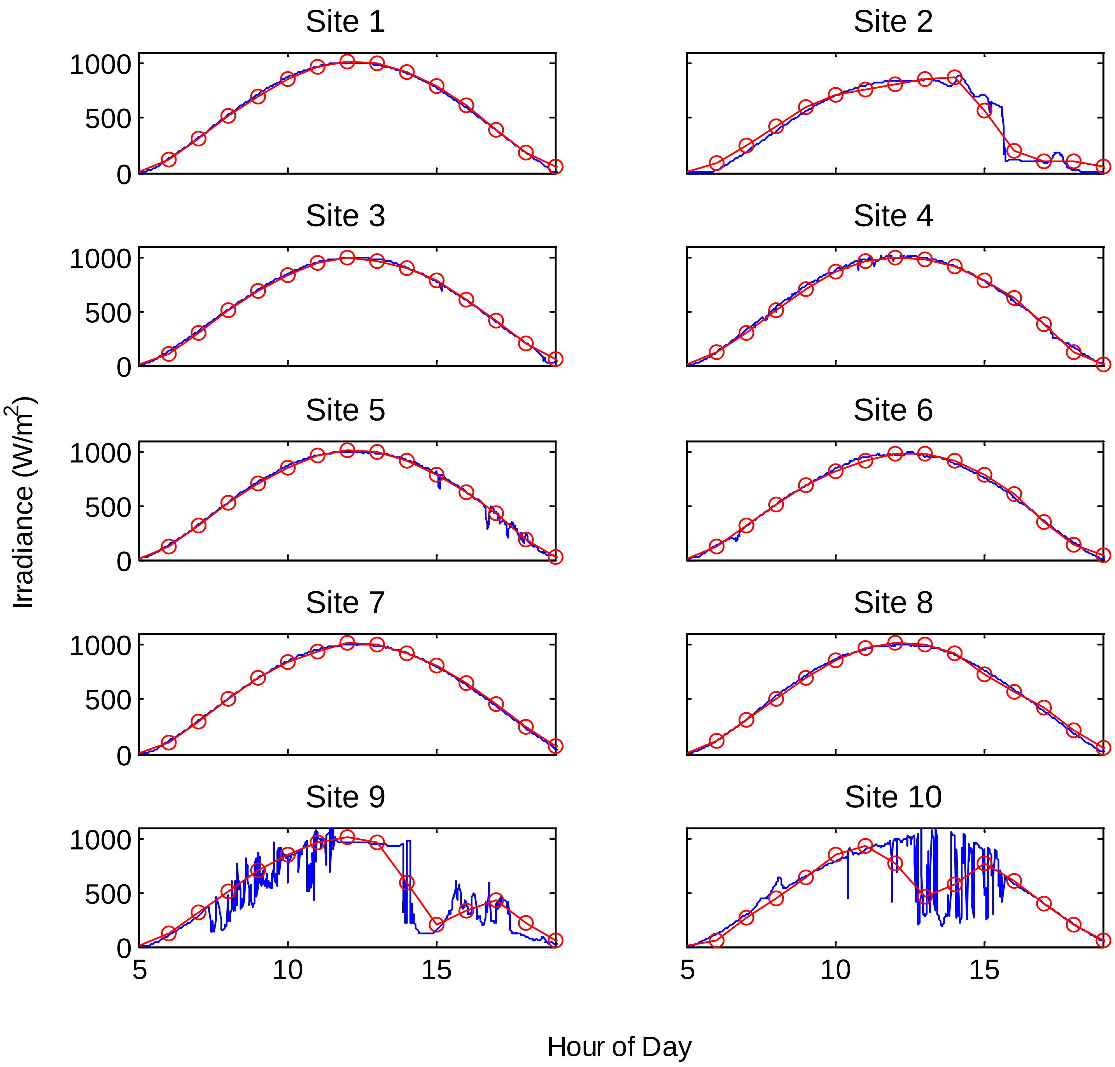

Figure 8. Estimated Irradiance at all Sites on Day 202.

Figure 9 shows the AC power at each site that corresponds to the irradiance displayed in Figure 8. Sites with single-axis tracking (i.e., Sites 1, 4, 6, 7 and 10) exhibit squarer shapes that do sites with fixed-tilt arrays.

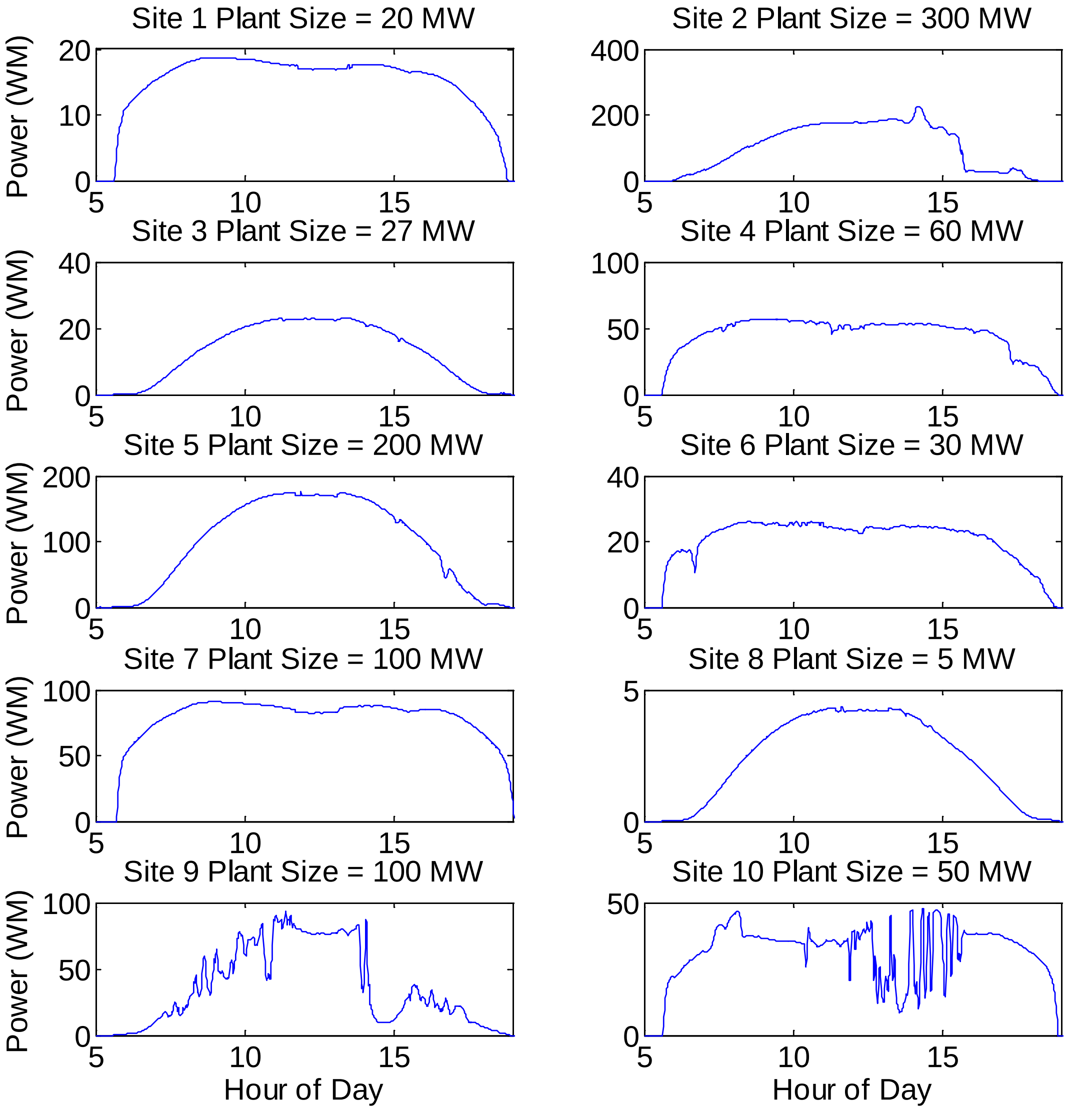

Figure 9. Estimated AC Power at all Sites on Day 202, Case 5.

3.2. Validation

Ideally, we would validate the simulation results by comparison with observations of irradiance and power during the time period of interest. However, neither irradiance sensors nor PV systems were operating at the sites of interest; consequently our validation effort focuses on comparing simulated irradiance with satellite estimates of irradiance and with ground measurements from the LVVWD sites. We examine statistical summaries of the simulation results in order to determine the extent to which simulation results are consistent with available data. We also examine our simulation results to see if patterns are present that have been observed in irradiance data collected within other regions.

3.2.1. Distributions of Irradiance

Figure 10 compares empirical cumulative distribution functions (CDFs) for the one-year time series of irradiance at one-minute intervals (resulting from the simulation) to the CDFs for the time series of hourly average irradiance estimated from satellite data. The CDF is formed by regarding the ensemble of irradiance values at each time step as equally likely elements of a sample. The very close agreement between simulation results and data, despite the difference in time step length, confirms that the irradiance levels in the simulation results occur at the same frequencies as are observed in the data. Consequently, using either the simulated one-minute time series of irradiance or the hourly values from the satellite data would produce similar CDFs of power at each site.

3.2.2. Distributions of Changes in Irradiance

Figure 11 compares the uppermost percentiles of the CDFs of changes in one-minute time series of irradiance (i.e., the absolute value of the difference in the values at consecutive minutes) between the simulated time series and the time series recorded at the LVVWD sites. Changes in irradiance correspond to changes in power from PV plants; analogously, the frequency at which irradiance changes occur corresponds to the frequency of changes in power output.

Figure 11 shows that the frequencies of large changes (as quantified by the highest percentiles of the CDFs of changes) in the simulation results are similar to those observed at the LVVWD sites. Changes in irradiance are due either to the movement of cloud shadows or to the diurnal solar pattern. The darkness, duration and intermittency cloud shadows at the ground surface are results of regional weather. Because both the study locations and the LVVWD measurement stations are located within a climatically similar region, characterized as arid basin-and-range topography, simulation results should exhibit similar changes in irradiance as are observed at measurement sites within the region. Figure 11 confirms that the simulation algorithm produces results that reasonably agree with measurements.

As indicated by satellite observations, Site 2 experienced about 5% less annual insolation than the LVVWD sites (determined by comparing satellite estimates to ground measurements), indicating that cloudy conditions occur more frequently at Site 2 than within the Las Vegas valley. Because hourly averages of irradiance are less than clear-sky values more frequently at Site 2, the simulation selects days with variable irradiance more often at Site 2 than occur at the LVVWD sites. Consequently, the CDF of changes in irradiance at Site 2 indicates more frequent, large ramps than occur at the LVVWD sites.

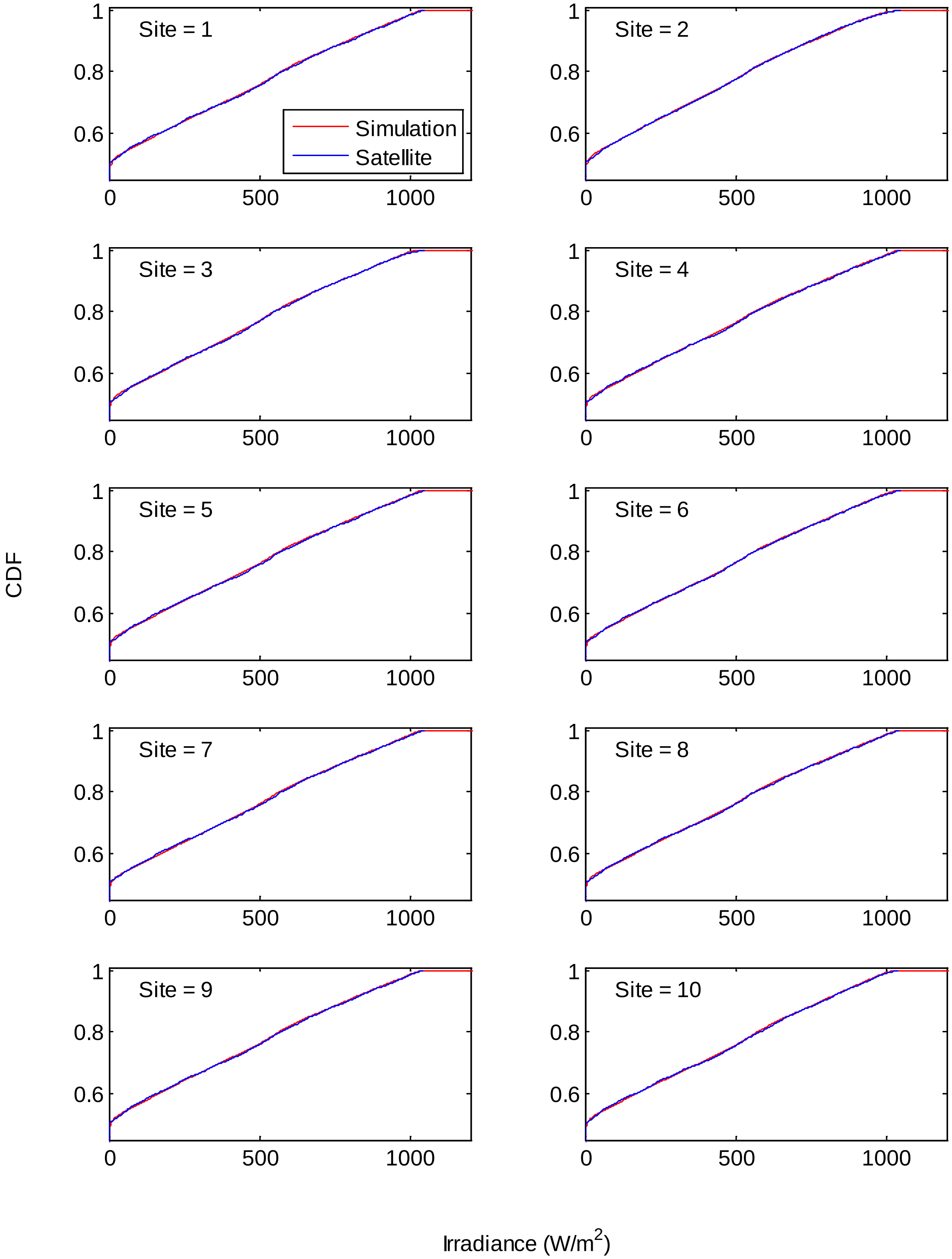

Figure 10. Comparison of CDFs of Annual Irradiance Between Simulated One-Minute Irradiance and Hourly Average Irradiance Estimated From Satellite Data.

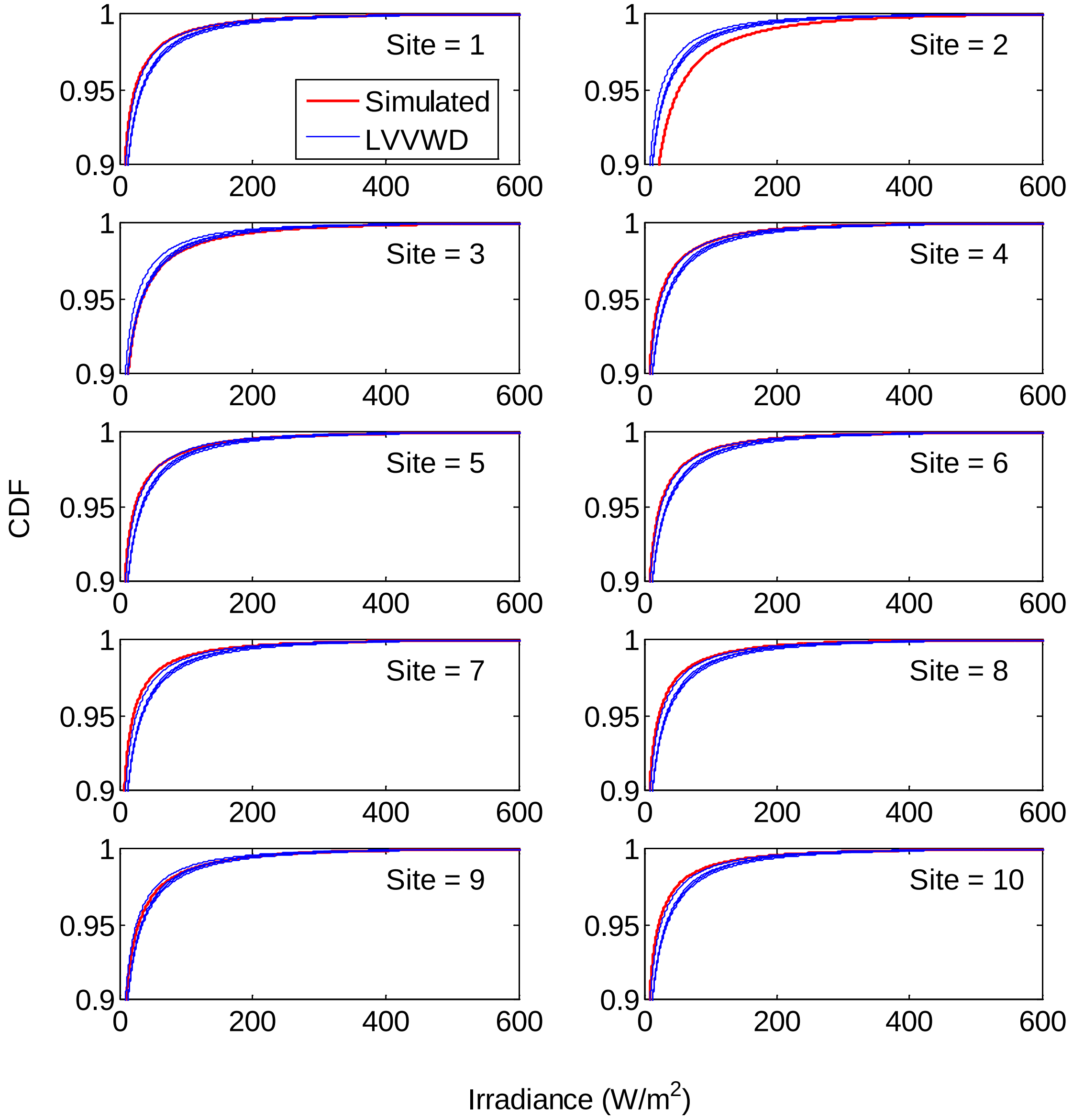

Figure 11. Comparison of CDFs of Changes in One-Minute Irradiance Between Simulations and LVVWD Data.

3.2.3. Correlations Between Changes in Irradiance

Time series of changes in irradiance can be examined for correlations between changes observed at different sites. Positive correlation coefficients indicate sites that generally experience concurrent increases or decreases in irradiance, whereas negative coefficients indicate generally opposite changes in irradiance changes. To remove diurnal effects, irradiance is scaled by its clear sky value; the resulting fraction is termed the clear sky index. Previous analyses of correlations in the changes in clear sky index values have shown that correlations are generally positive but decrease as the distance between sites increases, or as the time interval used to define irradiance changes decreases. Intuitively, these analyses indicate that changes in irradiance at widely separated sites are uncorrelated over short time scales.

We converted our one-minute time series of irradiance at each site to clear sky index (denoted by Kt) using clear sky irradiance that was estimated using a simple clear sky model developed by Atwood and Ball [22] This model expresses clear sky irradiance as a function of zenith angle, sky albedo, precipitable water, atmospheric pressure, ground albedo, and broadband aerosol optical depth. Zenith angle was determined from site latitude and longitude and time using a standard solar position algorithm. Table 4 shows the values used for the other parameters. We used the value for sky albedo provided by Atwood and Ball. For the remaining parameters, an uncertainty analysis showed that model results were most sensitive to the value of precipitable water. Consequently, this parameter's value was chosen to calibrate the clear sky model so that modeled irradiance agreed with irradiance measured during a selected set of clear days. Values were assumed for the remaining parameters, and model sensitivity was tested to ensure that model results were insensitive within an uncertain range about each assumed value. This approach is reasonable because the calculated clear-sky index is used indirectly to develop parameters that describe the day ahead forecasting error.

Table 4. Parameters and Values for Clear Sky Model

Parameter	Value	Source
Precipitable water	2.6 cm	Calibrated
Atmospheric pressure	950 mbar	Assumption
Ground albedo	0.2	Assumption
Sky albedo	0.0685	[22], p. 3
Broadband aerosol optical depth	0.05	Assumption

For each site, we computed time series of changes in the clear sky index, ΔK_t, by differencing clear sky index values separated by a fixed time interval T, i.e.,

$$\Delta K_t(\tau) = K_t(\tau) - K_t(\tau - T) \tag{6}$$

where $K_t(\tau)$ is the value of clear sky index at time τ. We then truncated each times series to the shortest common length and computed the Spearman correlation between the time series for each pair of sites. We also performed these calculations for clear sky index values at the LVVWD sites. Figure 12 displays the resulting correlation coefficients as a function of distance between site pairs and time interval T used to determine the difference. Solid markers indicate correlation coefficients for the LVVWD sites, and non-filled markers indicate values for the simulation sites.

Figure 12 shows the same general patterns as have been reported in analyses of irradiance measurements [23, Fig. 5]. Correlation coefficients generally decrease exponentially as distance increases. Correlations between simulation sites generally extend from the trend evident for the LVVWD sites, although for some time intervals (e.g., 60-minutes) the correlation coefficients for the simulation sites values decrease less rapidly as distance increases than do the correlation coefficients for the LVVWD sites. The reduction in the rate of decrease may be an artifact of the simulation method or may represent a characteristic of irradiance in the Las Vegas region. Some data show a similar feature (e.g., [24, Fig. 5]) but other data do not (e.g., [23, Fig. 5]).

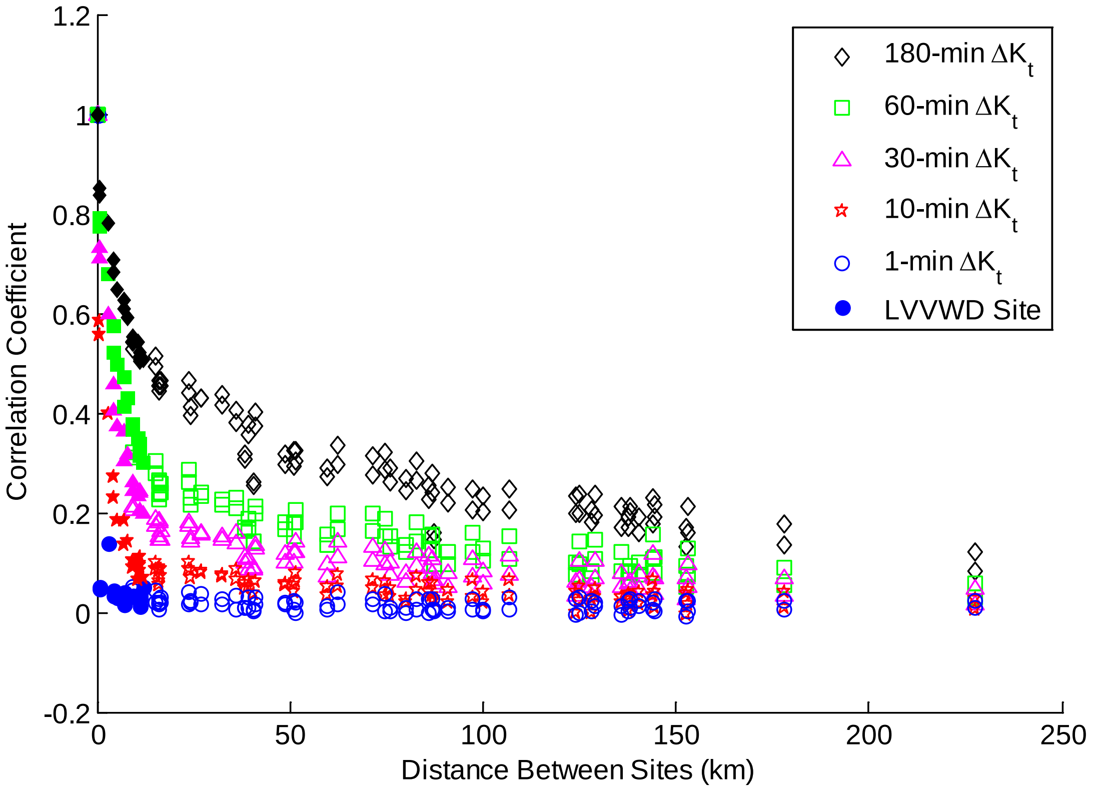

Figure 12. Correlations between Changes in Clear Sky Index (Kt) as a Function of Distance between Sites and Time Interval.

4. ANCILLARY ANALYSES

To support the NV Energy grid integration study, we prepared two data sets in addition to the one-minute time series of power from utility-scale plants: hourly time series of day-ahead forecasts of power from utility-scale plants; and one-minute time series of aggregate power from small (i.e., less than 2MW) commercial and residential roof-top PV systems distributed through the Las Vegas valley.

4.1. Day-ahead Forecasts

As part of the estimation of load following and regulation reserve requirements, NV Energy requested that Sandia National Laboratories provide day-ahead forecasts of hourly average power from each utility-scale plant, to accompany the one-minute time series of power output.

We reviewed literature describing forecasting methods and analyses of forecast performance and defined a method to emulate next-day forecasts of hourly average power at each plant with forecast errors consistent with current forecasting capabilities. Notably, Lorenz et al. [25] and Perez et al. [26] examine current forecasting methods, perform day-ahead forecasts of hourly irradiance forecasts, and report their forecast performance. Currently, the best documented performance of irradiance forecasts is achieved by combining numerical weather predictions (i.e., physics-based models) with various statistical methods that improve and correct model output based on historical data. However, because PV power output is nearly linear with irradiance, relative errors for irradiance forecasts are similar to those for power forecasts. Thus, reported performance for irradiance forecasts was used to emulate power forecasts.

The method used to produce day-ahead forecasts of hourly average power to accompany the simulated hourly average power for each site can be summarized as follows:

1. Assume that forecast models can reliably predict clear or partly cloudy conditions for the next day.
2. If clear conditions are predicted at the site, the relative forecast error (the ratio between the forecast value and the simulated power) is modeled as normally distributed with a mean of one. The standard deviation for the error distribution (0.035) is equal to the standard deviation of the ratio between hourly average irradiance measured at the LVVWD locations for clear days, and the hourly average irradiance projected by a clear sky model (as described in Section 3.2.3). One value for the relative forecast error is independently sampled for each clear day and each site and is multiplied by the simulated power to obtain the forecast for the site.
3. If cloudy conditions are predicted, the relative forecast error is randomly sampled for each hour from a normal distribution with a mean of zero, with an imposed correlation between values for successive hours. The standard deviation for the distribution of each hour's error depends on the hour's clear sky index, with values taken from [25, Fig. 5a]. Extreme values for the error (i.e., which would result in clear sky index values below 0.1 or above 1.2) are screened out and replaced by resampling. Forecast errors are determined independently for each PV plant; the relative forecast error for each hour added to the simulated power to produce the day-ahead power forecast.

The forecast emulation method, with its results, is described in detail in the remainder of this section.

Step 1: Classify each day of the year as clear or cloudy.

We assume that forecasting methods can reliably project whether the next day will be generally clear, or partly cloudy. We identify each day in 2007 as clear or cloudy, at each site, using irradiance estimated from satellite imagery of each site and a clear-sky model. We compare the total daily insolation from satellite data to that predicted by the clear sky model; days with total insolation within 8% of clear sky insolation are classified as clear; the remaining days are identified as cloudy. Figure 13 demonstrates the ability of the total insolation criteria to distinguish between clear and cloudy days. Figure 14 illustrates the occurrence of days identified as clear or cloudy throughout 2007. Figure 15 demonstrates ten days of simulated irradiance and the distinction between clear and cloudy days. Note that for days identified as clear, maximum irradiance varies somewhat between days, indicating that even when clear conditions are project, irradiance values retain some variability.

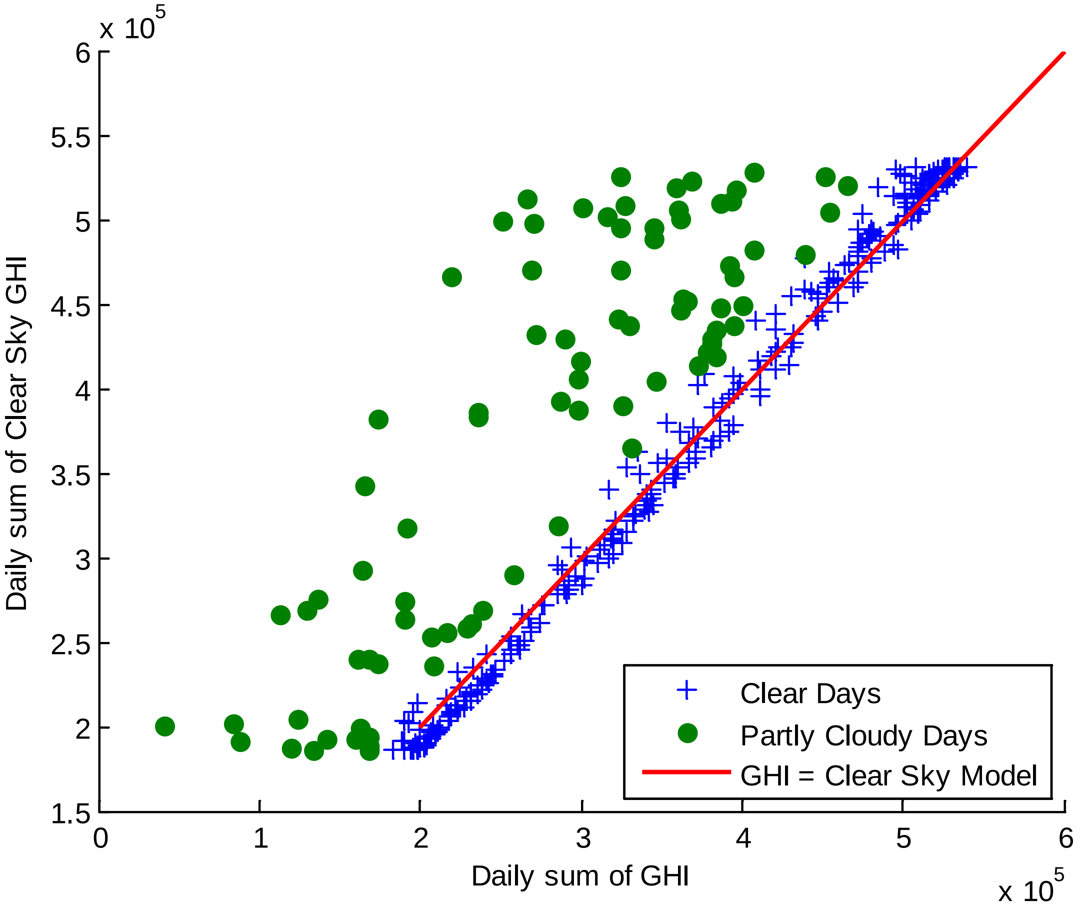

Figure 13. Identification of Clear and Cloudy Days.

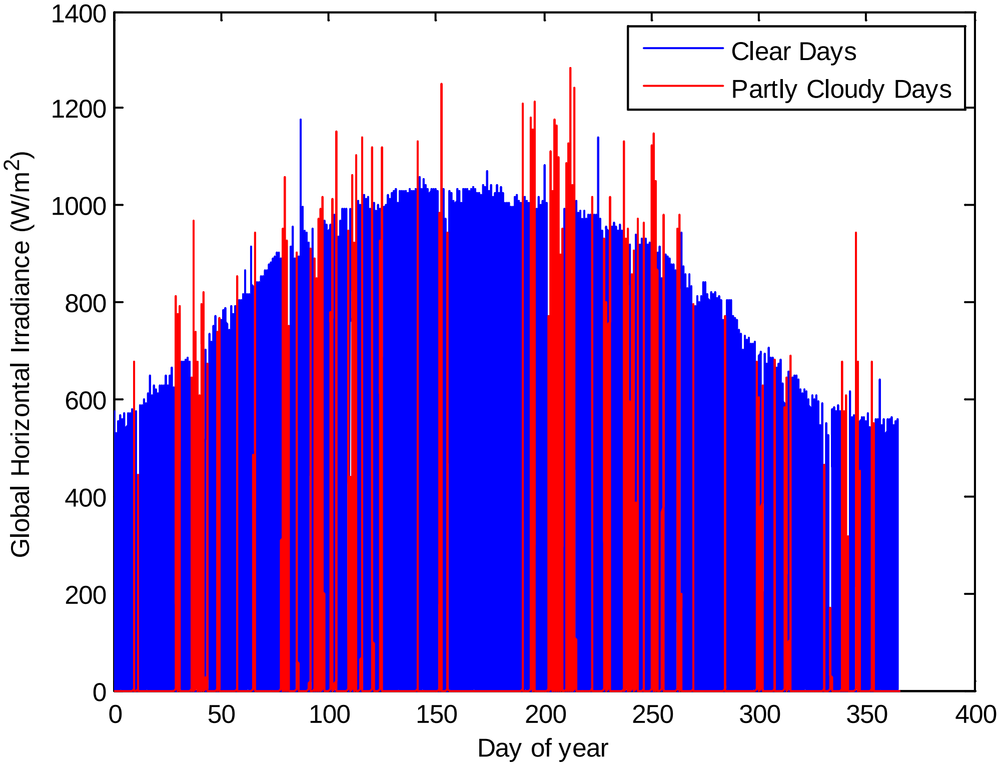

Figure 14. Occurrence of Clear and Cloudy Days in 2007.

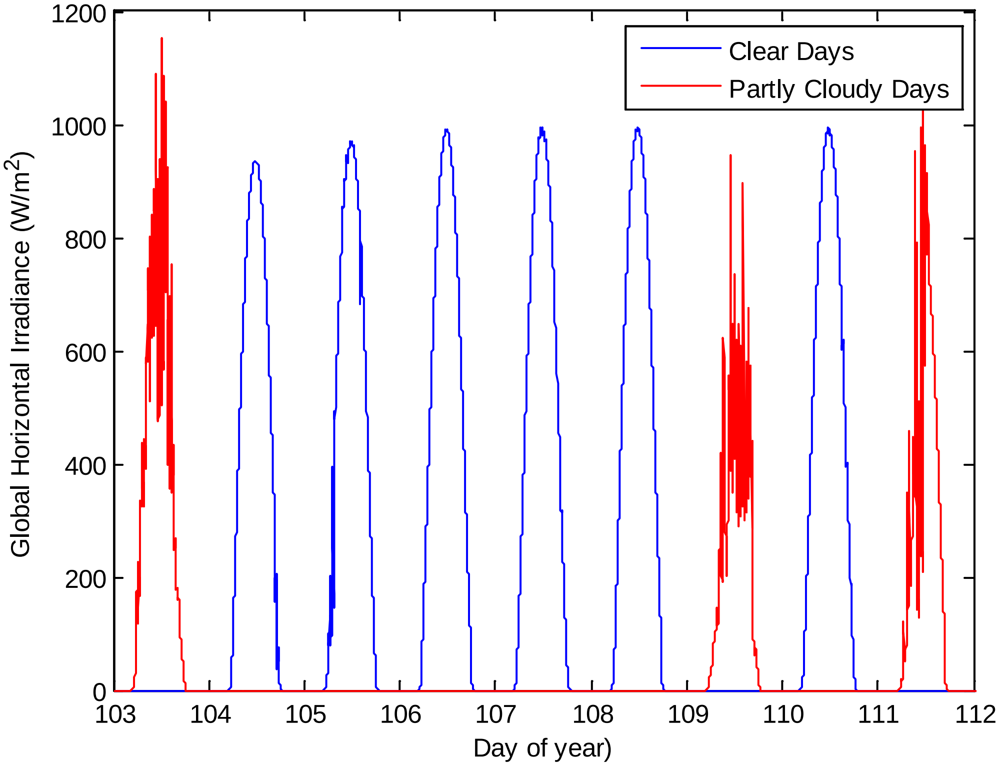

Figure 15. Irradiance Patterns on Clear and Cloudy Days.

Step 2: Generate forecast values for clear days.

Relative forecast error $\varepsilon(t)$ is defined as

$$\varepsilon(t)=\left(F(t)-I(t)\right)/I(t) \tag{7}$$

where $I(t)$ is the actual irradiance at time t and $F(t)$ is the forecast irradiance at the same time. On clear days, the relative forecast error is sampled once per day from a normal distribution with mean zero and standard deviation, denoted by σ_{Clr}, of 0.035. The value for σ_{Clr} was estimated from the standard deviation of the ratios of daily insolation from the LVVWD sites to the value estimated by the clear-sky model (see Section 3.2.3), for all clear days. Sampling of relative forecast errors is independent for each day and each site. To avoid extreme values for the forecast error, values for $\varepsilon(t)$ beyond three standard deviations are replaced by resampling. The hourly average power forecast $FP(t)$ for a clear day is then estimated by

$$FP(t)=\left(1+\varepsilon(t)\right)P(t) \tag{8}$$

where $P(t)$ is the power estimated by the algorithm outlined in Section 3 of this report. Figure 16 displays a histogram of the sampled relative forecast errors for clear days, along with the target normal distribution. Figure 16 confirms that the sample of relative forecast errors for clear days reproduces the selected distribution of relative error.

Step 3: Generate forecast values for cloudy days.

On cloudy days, forecast errors are sampled each hour, with correlation between successive hours, and the time series of forecast errors is generated independently for each site. The clear-sky model described in Section 3.2.3 of this report is used to compute a clear sky index for each hour of a cloudy day. The clear sky index is used to derive a standard deviation for the distribution of relative forecast error from Fig. 5a of Lorenz et al. [25]. Lorenz et al. [25] analyzed an irradiance forecast with reasonably good performance and presented relative error as a function of clear sky index in Fig. 5a of their paper. However, the relative errors they present are determined after the forecast values had been adjusted to remove biases and extreme values. We first generated a random sample of forecast errors from a normal distribution with mean zero and standard deviation as indicated in Fig. 5a of [25], then replaced extreme values (i.e., values that produced irradiance below 10% of clear-sky value, or above 120% of clear sky value) by resampling. The standard deviation of the resulting constrained sample (after removing extreme values) was significantly less than the target values in Fig. 5a of [25], indicating that a greater standard deviation should be used to generate the initial random sample. Accordingly, we increased the standard deviations at all clear sky index levels by 50%. Table 5 lists the standard deviation values we use to generate the relative forecast errors for cloudy days.

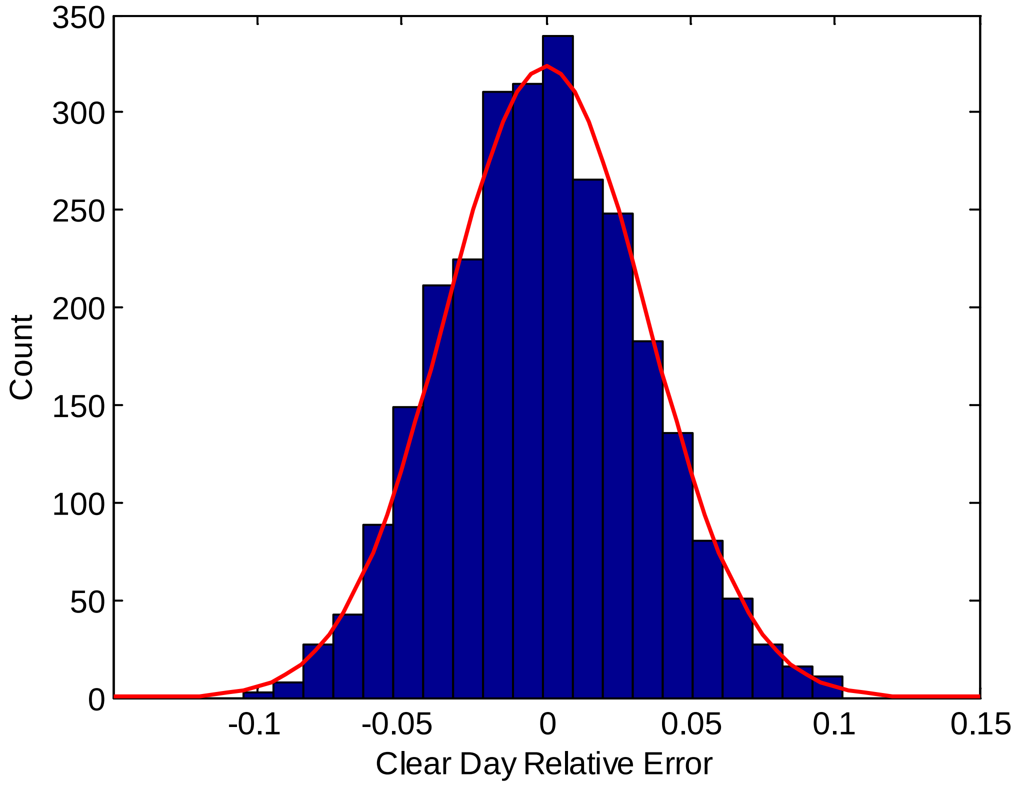

Figure 16. Sampled Relative Forecast Errors for Clear Days (blue) and Target Error Distribution (red).

Table 5. Standard Deviations Used to Generate Relative Forecast Errors for Cloudy Days.

Clear Sky Index Interval	Target Standard Deviation (from [25], Fig 5a)	Standard Deviation Used to Generate Forecast Errors
0.1 – 0.3	0.81	1.22
0.3 – 0.4	0.75	1.13
0.4 – 0.5	0.62	0.93
0.5 – 0.6	0.53	0.80
0.6 – 0.7	0.45	0.68
0.7 – 0.8	0.38	0.57
0.8 – 0.9	0.30	0.45
0.9 – 1.0	0.17	0.26
1.0 – 1.2	0.12	0.18

An initial sample of relative forecast errors is generated by first randomly sampling a value for the first hour of a cloudy day from a normal distribution with mean zero and standard deviation given in Table 5, using the average clear sky index value for the first hour. Values for successive values are then generated from normal distributions with zero mean and standard deviation from Table 5, but are correlated (with a value of 0.8) to the relative forecast error for the preceding hour. The correlation between successive hours represents the intuitive judgment that forecast errors are not random from hour to hour, but rather, would tend to stay above (or below) the actual values for some length of time before being corrected.

Extreme values of relative error (i.e., values that would result in clear sky index values less than 0.1 or greater than 1.2) are removed from the initial sample by resampling. The time series of relative forecast error is generated independently for each site. The hourly average power from each site for cloudy days is then computed by Eq. 8. Figure 17 compares the relative RMSE of forecast values of average hourly power during cloudy days to the average hourly power estimated for five sites, with the target relative RMSE values from Fig. 5a of [25]. The emulation method produces forecast errors that compare favorably to the results reported in [25].

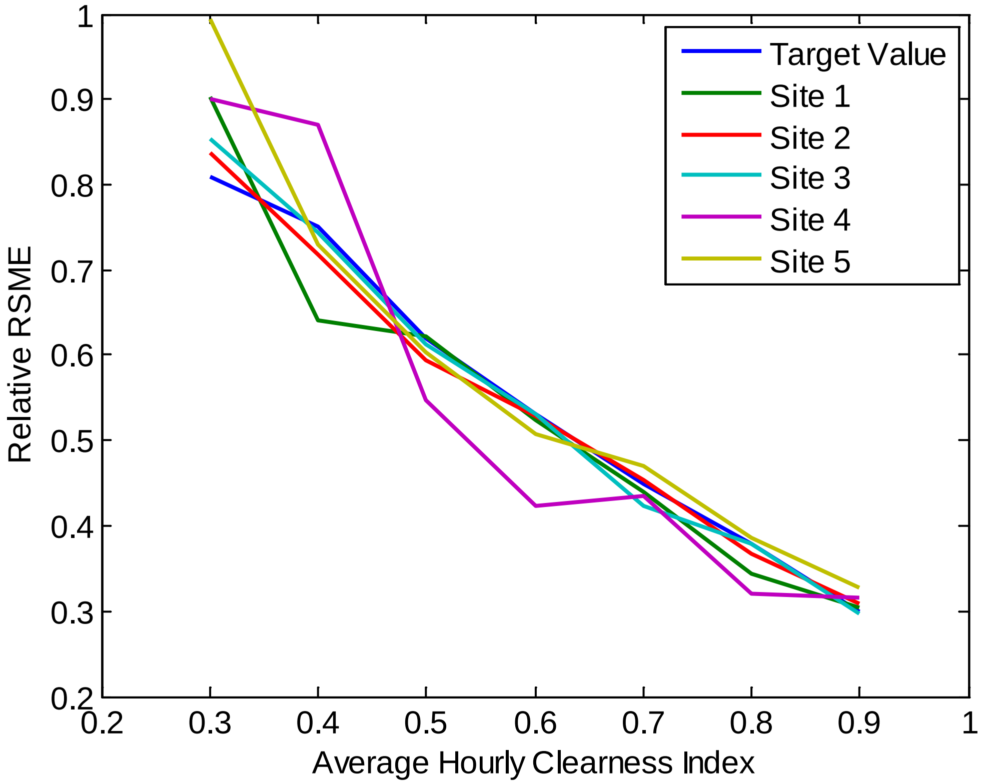

Figure 17. Forecast Error for Cloudy Days as a Function of Clear Sky Index.

The time series of forecast error (concatenating clear and cloudy days to an annual time series) can be applied to simulated GHI (rather than to simulated power) to produce an emulated day-ahead irradiance forecast. Figure 18 illustrates the simulated hourly GHI irradiance for six days, with the accompanying irradiance forecast. Curves appear relatively smooth because the hourly values are connected by straight line segments. The greater range of errors on cloudy days is apparent (e.g. days-of-year 201 and 206) whereas day-of-year 204 shows that forecast errors are generally smaller for clear days.

Perez et al. [26] have compared day-ahead forecasts of hourly irradiance to ground measurements at Desert Rock, NV. Figure 19 demonstrates that the relationship between our emulated forecast irradiance and our simulated irradiance is similar to the relationship between an actual irradiance forecast and measured irradiance at Desert Rock, NV (as reported in [26]).

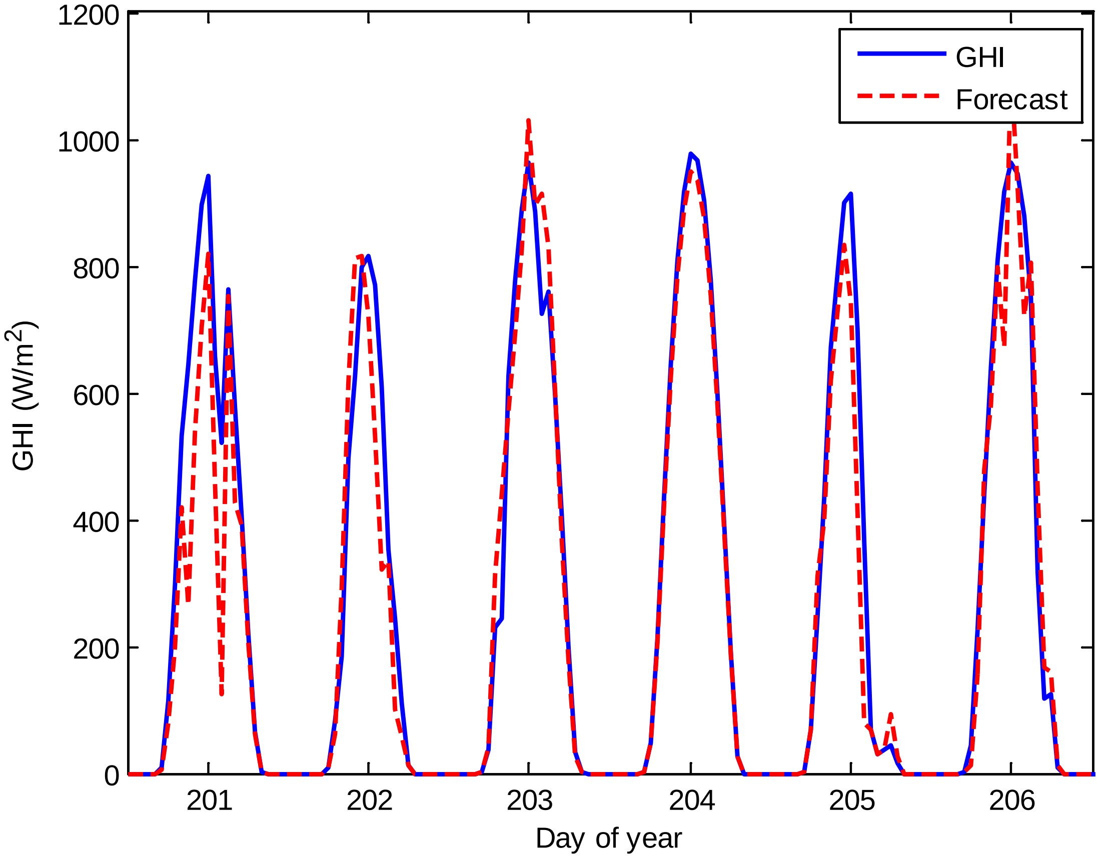

Figure 18. Comparison of Simulated Irradiance to Day-Ahead Forecast.

4.2. Power from Distributed PV Systems

We estimated a one-minute time series of aggregate power from small commercial (i.e., 3MW$_{AC}$ or less) and residential PV systems distributed through the Las Vegas valley, collectively referred to a distributed generation (DG) PV. The ensemble of systems comprising DG PV is summarized in Table 6; cases are defined by the percentage of total NV Energy generating capacity represented by DG PV.

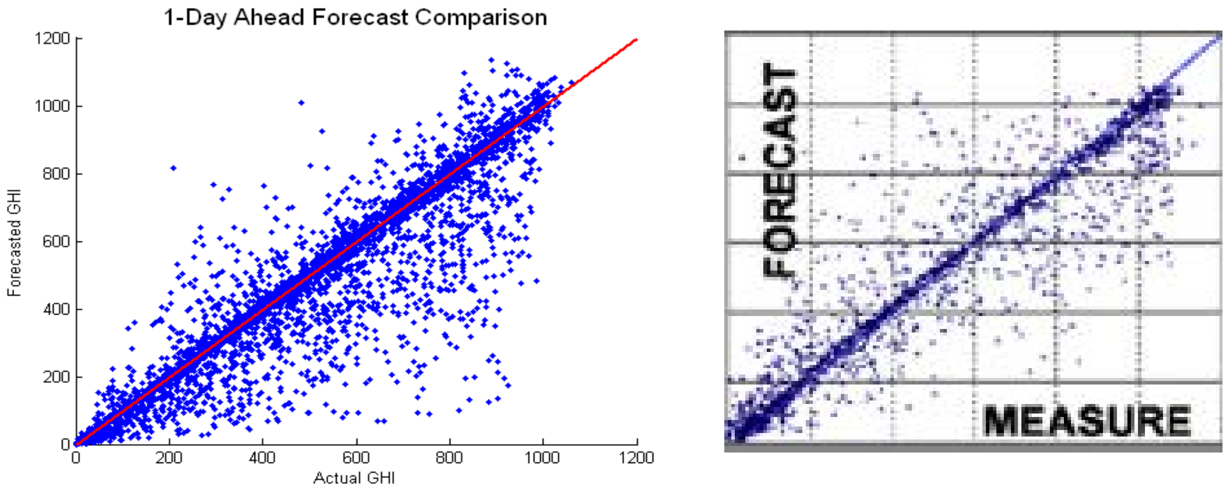

Figure 19. Comparison of Actual and Forecast GHI: Emulated Forecast (left) and Numerical Weather Model-Based Forecast for Desert Rock, Nevada (right).

Table 6. Summary of Distributed Generation PV Cases.

	Residential	**Commercial Rooftop**	**Commercial Ground Mount**
Description	4 kW_{AC} fixed tilt	300 kW_{AC} flat roof mount	3 MW_{AC} single-axis tracker
Case			
1%	42 MW	7 MW	7 MW
9%	378 MW	63 MW	63 MW
15%	630 MW	105 MW	105 MW

Residential systems are assumed to be made up of crystalline Si modules in 2 strings of 10 Yingli Solar YL230-29b modules each (the same modules assumed for the utility-scale, fixed tilt plants). We assumed that one 4kW_{AC} SMA SB4000US inverter is used. Systems are equally divided into five groups with different roof pitches: 4/12, 5/12, 6/12, 7/12 and 8/12. All systems are oriented toward the south.

Commercial rooftop systems are assumed to comprise Yingli Solar YL230-29b modules in a horizontal orientation, with three SatCon AE-30-60-OV-F 100 kW_{AC} inverters. Commercial ground mount systems also use Yingli Solar YL230-29b modules on single-axis trackers at latitude tilt, with six SatCon PVS-500 500kW_{AC} inverters.

Systems are assumed to be randomly distributed throughout the Las Vegas valley, which is approximately 1,500 km^2. Aggregate power from the ensemble of systems is estimated using the Sandia Array Performance Model [3], the spatial average of irradiance over the Las Vegas valley, and temperature and wind speed from McCarran International Airport. We estimated the spatial average of GHI over the Las Vegas valley by averaging GHI measured at the six LVVWD stations, and then smoothing the resulting time series by computing a ten-minute moving average. Because the variability in the simple average of the LVVWD data (without any temporal averaging) is representative of the aggregate power from a few discrete systems, rather than hundreds of systems, we judged it appropriate to further smooth the average by using a temporal average with a time window commensurate with the time for a cloud shadow to transit the length of the Las Vegas valley. Figure 20 illustrates one week of estimated power from DG PV. Power closely follows the estimated ten-minute temporal average of irradiance over the Las Vegas valley, which is approximated by the average over the six LVVWD irradiance measurements. At night, power is estimated to be slightly negative reflecting the implicit load presented by the DG systems' inverters, which remain connected to the grid and consume a slight amount of power.

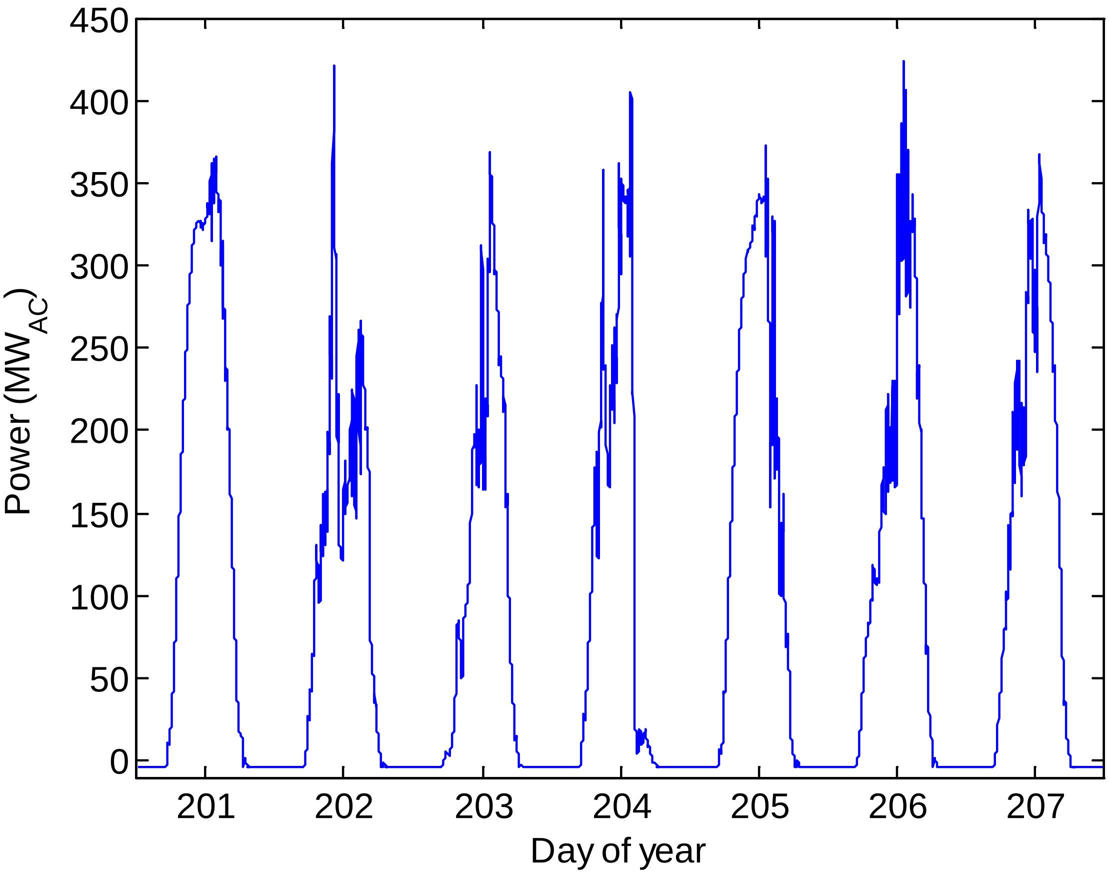

Figure 20. One Week of Estimated Power from Distributed Generation PV.

We also produced a day-ahead forecast of hourly DG PV power, using the method outlined in Section 4.2, but reducing the standard deviations of the distributions of forecast error by 25% from the values listed in Table 5. Lorenz et al. [25] examine the reduction in forecast errors achieved when forecasts are aggregated over regions of increasing size. For an area approximately 0.5°×0.5° (roughly the size of the Las Vegas valley), their results show a reduction in relative forecast error of about 25%. We assumed a similar reduction could be achieved for a forecast of aggregate irradiance over the Las Vegas valley, as opposed to a location within the valley.

4. REFERENCES

1. Public Utility Commission of Nevada, Docket 10-02009, Granted Order dated 7/30/2010, Section W.
2. Navigant Consulting, Inc, *Large-Scale PV Integration Study*, Burlington, MA, July 30, 2011
3. King, D. L., W. E. Boyson, J. A. Kratochvill, *Photovoltaic Array Performance Model*, SAND2004-3535, Albuquerque, NM, Sandia National Laboratories, 2004
4. Kuszmaul, S., A. Ellis, J. Stein, L. Johnson, *Lanai High-Density Irradiance Sensor Network for Characterizing Solar Resource Variability of MW-Scale PV System*, 35th IEEE PVSC, Honolulu, HI, 2010
5. Clean Power Research SolarAnywhere website: https://www.solaranywhere.com
6. Perez, R., Ineichen, P., Moore, K., Kmiecik, M., Chain, C., George, R., and Vignola, F, *A New Operational Satellite-to-Irradiance Model*, Solar Energy 73(5), pp.307-317, 2002
7. Stein, J., R. Perez, A. Parkins, *Validation of PV Performance Models using Satellite-Based Irradiance Measurements: A Case Study*, SOLAR2010, Phoenix, AZ, 2010
8. Perez, R., J. Schlemmer, D. Renne, S. Cowlin, R. George, B. Bandyopadhyay, *Validation of the SUNY Satellite Model in a Meteosat Environment*, Proc., ASES Annual Conference, Buffalo, NY, 2009
9. Stackhouse, P., T. Zhang, W. S. Chandler, C. H. Whitlock, J. M. Hoell, D. J. Westberg, R. Perez, S. Wilcox, *Satellite Based Assessment of the NSRDB Site Irradiances and Time Series from NASA and SUNY/Albany Algorithms*, Proc. ASES Annual Meeting, San Diego, CA, 2008
10. Glasbey, C. A., *Nonlinear autoregressive time series with multivariate Gaussian mixtures as marginal distributions,* Applied Statistics 50: 143-154, 2001
11. Skartveit, A. and J. A. Olseth, *The probability density and autocorrelation of short-term global and beam irradiance*, Solar Energy 49(6) pp. 477-487, 1992
12. Tovar, J., F. J. Olmo, L. Alados-Arboledas, *One-minute global Irradiance probability density distributions conditioned to the optical air mass*, Solar Energy 62(6): 387-393, 1998
13. Tovar, J., F. J. Olmo, F. J. Batlles, L. Alados-Arboledas, *One-minute* k_b *and* k_d *probability density distributions conditioned to the optical air mass*, Solar Energy 65(5), pp. 297-304, 1999
14. Tovar, J., F. J. Olmo, F. J. Batlles, L. Alados-Arboledas, *Dependence of one-minute global irradiance probability density distributions on hourly irradiation*, Energy 26, pp. 659-668, 2001
15. Tovar-Pescador, J., *Modelling the Statistical Properties of Solar, Radiation and Proposal of a Technique Based on Boltzmann Statistics*, in Modeling Solar Radiation at the Earth's Surface: Recent Advances, ed. V. Badescu. Berlin, Springer-Verlag, pp. 55-91, 2008
16. Longhetto, A., G. Elisei, C. Giraud, *Effect of correlations in time and spatial extent on performance of very large solar conversion systems,* Solar Energy 43(2), 77-84, 1989
17. Data obtained from University of Wyoming College of Engineering web service: http://weather.uwyo.edu/upperair/sounding.html Desert Rock station number is 72387.
18. Maxwell, E. L., *A Quasi-Physical Model for Converting Hourly Global Horizontal to Direct Normal Insolation*. Golden, CO, Solar Energy Research Institute, 1987
19. Chang, T. P., *The gain of single-axis tracked panel according to extraterrestrial radiation*, Applied Energy 86, pp. 1074-1079, 2009

20. Perez, Richard; Ineichen, Pierre; and Seals, Robert, *Modeling Daylight Availability and Irradiance Components from Direct and Global Irradiance*, Solar Energy 44(5), pp. 271-289, 1990
21. King, D. l., S. Gonzalez, G. M. Galbraith, W. E. Boyson, SAND2007-5036, *Performance Model for Grid-Connected Photovoltaic Inverters*, Sandia National Laboratories, Albuquerque, NM, 2007
22. Bird, R.E., Hulstrom, R., SERI/TR-642-761, *A Simplified Clear Sky Model for Direct and Diffuse Insolation on Horizontal Surfaces*, Solar Energy Research Institute, Golden, CO, 1981.
23. Mills, A. and R. Wiser, *Geographic Diversity for Short-Term Variability of Solar Power*, LBNL-3884E, Lawrence Berkeley National Laboratory, Berkeley, CA, Sept. 2010.
24. Hoff, T. and R. Perez, *Modeling PV Fleet Output Variability* (Draft), Clean Power Research, Napa, CA, May 2011.
25. Lorenz, E. *Irradiance Forecasting for the Power Prediction of Grid-Connected Photovoltaic Systems*, IEEE Jour. of Sel. Topics in Appl. Earth Obs. And Remote Sensing, Vol 2 pp. 2-10, Mar. 2009.
26. Perez, R., S. Kivalov, J. Schlemmer, K. Hemker Jr., D. Renne, T. E. Hoff, *Validation of Short and Medium Term Operational Solar Radiation Forecasts in the US,* Solar Energy 84, pp. 2161-2172, 2010.

DISTRIBUTION

1	MS0899	Technical Library	9536 (electronic copy)

Sandia National Laboratories